

Single-cell and spatial transcriptomics reveal somitogenesis in gastruloids

<https://doi.org/10.1038/s41586-020-2024-3>

Received: 4 December 2018

Accepted: 19 December 2019

Published online: 19 February 2020

 Check for updates

Susanne C. van den Brink^{1,6}, Anna Alemany^{1,6}, Vincent van Batenburg^{1,6}, Naomi Moris², Marloes Blotenburg¹, Judith Vivié¹, Peter Baillie-Johnson², Jennifer Nichols^{3,4}, Katharina F. Sonnen⁵, Alfonso Martinez Arias² & Alexander van Oudenaarden¹

Gastruloids are three-dimensional aggregates of embryonic stem cells that display key features of mammalian development after implantation, including germ-layer specification and axial organization^{1–3}. To date, the expression pattern of only a small number of genes in gastruloids has been explored with microscopy, and the extent to which genome-wide expression patterns in gastruloids mimic those in embryos is unclear. Here we compare mouse gastruloids with mouse embryos using single-cell RNA sequencing and spatial transcriptomics. We identify various embryonic cell types that were not previously known to be present in gastruloids, and show that key regulators of somitogenesis are expressed similarly between embryos and gastruloids. Using live imaging, we show that the somitogenesis clock is active in gastruloids and has dynamics that resemble those in vivo. Because gastruloids can be grown in large quantities, we performed a small screen that revealed how reduced FGF signalling induces a short-tail phenotype in embryos. Finally, we demonstrate that embedding in Matrigel induces gastruloids to generate somites with the correct rostral–caudal patterning, which appear sequentially in an anterior-to-posterior direction over time. This study thus shows the power of gastruloids as a model system for exploring development and somitogenesis in vitro in a high-throughput manner.

It has previously been shown that transcriptomes of entire gastruloids at 120 h after aggregation resemble that of mouse embryos at embryonic day (E)8.5 (ref. ³). To extend this characterization to the single-cell level, we applied single-cell RNA sequencing (scRNA-seq) to 25,202 cells obtained from 100 gastruloids at 120 h after aggregation that were generated using the mouse embryonic stem (ES) cell lines E14-IB10 or LfngT2AVenus (Extended Data Fig. 1a, b, Methods), and clustered cells on the basis of highly variable genes (Fig. 1a, Extended Data Fig. 1c–f, Supplementary Tables 1, 2). To annotate the 13 resulting clusters, we compared their transcriptomes to a scRNA-seq dataset from E8.5 mouse embryos⁴ (Extended Data Fig. 1g, h, Methods, Supplementary Table 3). We confirmed previous reports^{1,3} of the absence of anterior neuronal cell types and the presence of ectodermal cells that resemble embryonic spinal cord (cluster 8) (Extended Data Figs. 1g–i, 2). Additionally, we identified endothelial and haemato-endothelial cells (cluster 10), and found a cluster of cells with signatures of primordial germ cells and extra-embryonic ectoderm (cluster 12) (Extended Data Fig. 1i). Cluster 13 correlates with the visceral endoderm; however, we suggest that this cluster represents definitive endoderm, because previous studies have shown that visceral endoderm has been incorporated into definitive endoderm in mouse embryos by E8.5 (refs. ^{5,6}). We find the olfactory-receptor genes *Olfir959* and *Olfir129* upregulated in cluster 9, which suggests the presence of sensory neuron precursors. This

cluster also expresses markers linked to head mesenchyme, pharyngeal pouches, branchial arches and neural crest, and correlates with mesenchyme in embryos. Cluster 11 might represent allantoic cells, as it expresses *Tbx4* (which in E8.5 embryos is found exclusively in the allantois^{4,7}). A comparison between both ES cell lines revealed that some cell types are more prevalent in one of the two lines (Extended Data Fig. 1e, Supplementary Tables 1, 4), which indicates that genetic background can skew the cell-type composition of gastruloids.

While exploring cells in clusters 1–8, we observed that these cells are ordered along neural and mesodermal differentiation trajectories. To further explore this, we plotted the expression of genes linked to neural and mesodermal differentiation processes along clusters 1–8 (Extended Data Fig. 2b, d, Methods). First, we observed a neuromesodermal progenitor-to-neural differentiation trajectory from cluster 7 to cluster 8 that starts with the expression of the tail-bud genes *T* (also known as *Brachyury*), *Nkx1-2* and *Cyp26a1*, and is followed by the expression of neural differentiation markers such as *Sox2*, *Hes3*, *Sox1* and *Pax6*⁸. Second, we observed a mesodermal differentiation trajectory from cluster 6 to cluster 2. Consistent with what happens in embryos, the expression levels of tail-bud and FGF/WNT signalling genes (*Fgf8*, *Fgf17* and *Wnt3a*) decline in cells that differentiate towards a presomitic fate (characterized by the expression of *Tbx6* and *Hes7*⁹), with expression levels being lower in the somite differentiation front (which expresses

¹Oncode Institute, Hubrecht Institute-KNAW (Royal Netherlands Academy of Arts and Sciences) and University Medical Center Utrecht, Utrecht, The Netherlands. ²Department of Genetics, University of Cambridge, Cambridge, UK. ³Wellcome Trust–Medical Research Council Cambridge Stem Cell Institute, University of Cambridge, Cambridge, UK. ⁴Department of Physiology, Development and Neuroscience, University of Cambridge, Cambridge, UK. ⁵Hubrecht Institute-KNAW (Royal Netherlands Academy of Arts and Sciences) and University Medical Center Utrecht, Utrecht, The Netherlands. ⁶These authors contributed equally: Susanne C. van den Brink, Anna Alemany, Vincent van Batenburg. [✉]e-mail: s.c.vandenbrink@gmail.com; a.vanoudenaarden@hubrecht.eu

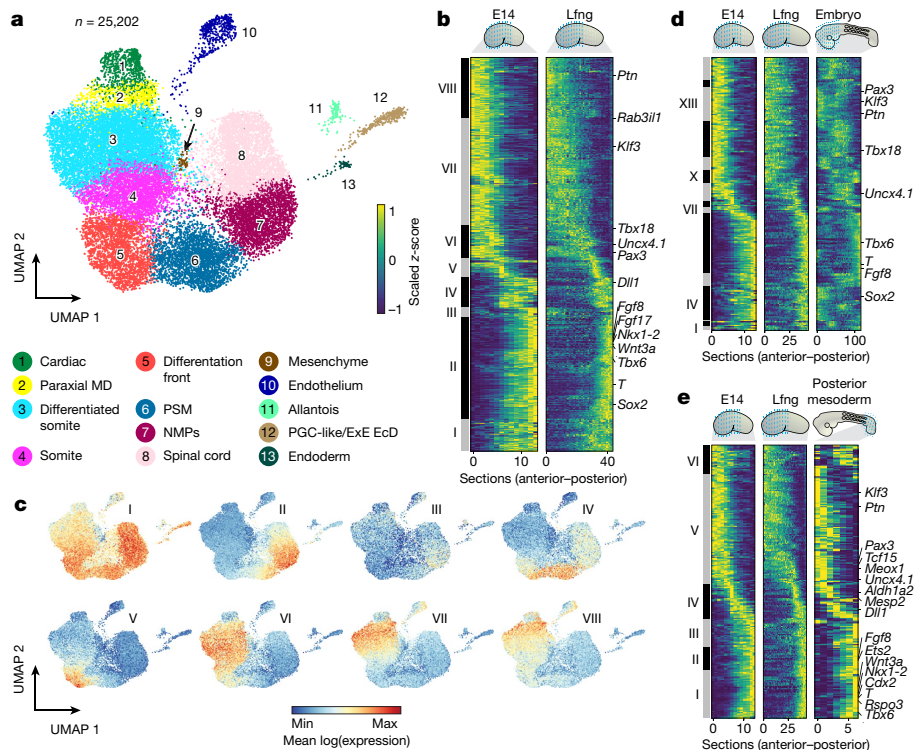


Fig. 1 | scRNA-seq and tomo-seq on mouse gastruloids and comparison to embryos. **a**, UMAP plot showing $n = 25,202$ cells isolated from 120-h gastruloids ($n = 26$ and 74 biologically independent gastruloids grown using E14-IB10 and LfngT2AVenus (ref.¹⁵) ES cell lines, respectively; $n = 6$ independent experiments) cultured in standard^{1,20} conditions. Cells are coloured and numbered by their cluster annotation. **b**, Heat map showing the average anterior–posterior expression pattern of 514 genes detected by tomo-seq¹¹ in 120-h gastruloids generated from E14-IB10 and LfngT2AVenus¹⁵ mouse ES cells using standard^{1,20} culture protocols. Only genes reproducible between all E14-IB10 ($n = 5$ biological replicates) and LfngT2AVenus ($n = 3$ biological replicates) gastruloids are shown (Methods). Genes are clustered (clusters I–VIII) based on their anterior–posterior expression pattern

(Supplementary Tables 5, 6, Methods). **c**, Mean log expression of genes present in each tomo-seq cluster from **b** plotted on the UMAP plot ($n = 43, 132, 13, 39, 26, 42, 141$ and 78 genes for clusters I, II, III, IV, V, VI, VII and VIII, respectively).

d, e, As in **b**, but showing 222 (**d**) or 239 genes (**e**) found to be reproducible (Methods) between $n = 5$ biological replicates of E14-IB10 and $n = 3$ biological replicates of LfngT2AVenus gastruloids, and E8.5 mouse embryos ($n = 3$ biological replicates) (**d**) or posterior mesoderm of E9.5 mouse embryos¹² ($n = 3$ biological replicates) (**e**). E14, E14-IB10; ExE, extra-embryonic; EcD, ectoderm; Lfng, LfngT2AVenus; MD, mesoderm; NMPs, neuromesodermal progenitors; PGC, primordial germ cells; PSM, presomitic mesoderm. Blue dashed lines refer to anterior–posterior sectioning of gastruloids or embryos during the tomo-seq procedure.

Ripply2). Upon somitic differentiation, cells first express *Uncx4.1* (also known as *Uncx*) and *Tbx18*, and later express markers of more-differentiated somites such as *Meox2* and *Pax3*⁹ (Extended Data Fig. 2d). Finally, cluster I expresses heart markers (*Gata6* and *Hand2*¹⁰).

In embryos, neural and mesodermal differentiation trajectories have a strong spatial component: neuromesodermal progenitors are located within the tail bud, and differentiated tissues are located more anteriorly⁸. To determine whether this is also the case in gastruloids, we applied RNA tomography (tomo-seq¹¹), a spatial transcriptomics technology, to 120-h E14-IB10 and LfngT2AVenus gastruloids (Extended Data Figs. 3–5, Methods). In these experiments, gastruloids were cryosectioned along their anterior–posterior axis, after which the mRNA content of the sequential sections was sequenced (Methods). For each cell line, we selected reproducible genes between replicates, and clustered these according to their anterior–posterior expression pattern (Methods, Supplementary Tables 5, 6; tomo-seq clusters are referred to with Roman numerals). The overall gene-expression patterns between gastruloids generated from the two ES cell lines are similar to one another (Fig. 1b, Extended Data Figs. 5, 6, Supplementary Tables 6–8). To annotate the various expression domains, we projected the mean expression of the genes in each tomo-seq cluster onto the uniform manifold approximation and projection (UMAP) plot (Fig. 1c). This revealed that neuromesodermal progenitors (cluster 7 in Fig. 1a; cluster II in Fig. 1b) are located in the most-posterior part of the gastruloids. More-differentiated neural cells are found slightly more anteriorly (Extended Data Fig. 3e). Furthermore, mesodermal clusters in the

UMAP plot are sequentially ordered along the anterior–posterior axis of gastruloids: cluster 6 (which roughly corresponds to cluster IV in tomo-seq) is the most posterior, and cluster 2 (which roughly corresponds to cluster VIII in tomo-seq) the most anterior (Fig. 1b, c, Extended Data Fig. 3e). This revealed that the neural and mesodermal differentiation trajectories in gastruloids are linked to their anterior–posterior axis, which is consistent with what occurs in embryos^{8,9}. Additionally, we found that the anterior domain in gastruloids (clusters VI, VII and VIII) contains cardiac, endothelial and head mesenchymal cells (Fig. 1b, c, Extended Data Fig. 3e). This is consistent with the locations of these tissues in embryos.

To further investigate the extent to which anterior–posterior gene-expression patterns in gastruloids recapitulate those in embryos, we applied tomo-seq to E8.5 mouse embryos (Fig. 1d, Extended Data Figs. 3–6, Methods, Supplementary Tables 5–8). This revealed that mesoderm genes, including genes that regulate somitogenesis, are expressed very similarly between embryos and gastruloids. We detected cardiac and brain domains in embryos (clusters VII and I, respectively, in Extended Data Fig. 5b) that are not clearly defined and absent, respectively, in gastruloids. Additional differences and similarities between embryos and gastruloids are presented in Extended Data Fig. 5, Supplementary Tables 7, 8, and visualization is provided at <https://avolab.hubrecht.eu/MouseGastruloids2020>. We also compared our gastruloid tomo-seq dataset to a previously published microarray dataset in which the posterior mesoderm (from the tail bud to the newly formed somite) of E9.5 mouse embryos was dissected into 7 anterior–posterior regions

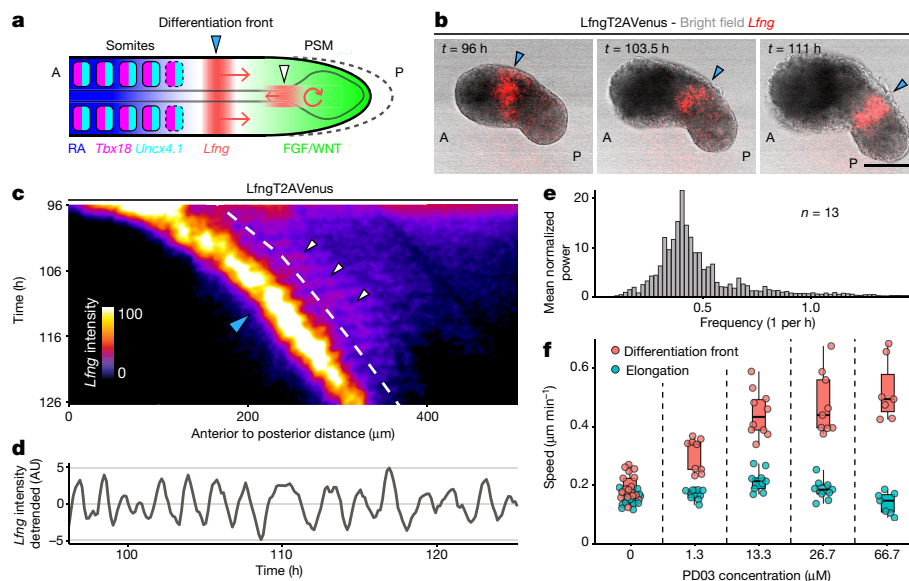


Fig. 2 | Time-lapse imaging and perturbation of the segmentation clock in mouse gastruloids. **a**, Illustration of somitogenesis in mouse embryos. Dark blue, retinoic acid (RA) gradient; red area and arrows, dynamic expression of *Lfng*; green, FGF/WNT signalling gradient in presomitic mesoderm; magenta and cyan blocks, somites; blocks with dotted lines, newly forming somites; posterior dotted line, posterior elongation of the presomitic mesoderm. **b**, Representative example of imaging of a *LfngT2AVenus*¹⁵ gastruloid embedded in 100% Matrigel at 96 h and subsequently imaged for 17 h (Supplementary Video 1). Blue arrowheads show the anterior–posterior displacement of the differentiation front (red, *Lfng*-expressing). Similar results were obtained in $n = 9$ independent experiments. **c**, Representative example of kymograph along the anterior–posterior axis of a *LfngT2AVenus* gastruloid embedded in 100% Matrigel at 96 h and subsequently imaged for 30 h. Similar

results were obtained in $n = 5$ independent experiments. Highest-intensity signal reflects the posteriorly moving differentiation front (blue arrowhead in **b**); white arrowheads indicate periodic oscillations in the presomitic mesoderm. **d**, Detrended *LfngT2AVenus* intensity along the dashed white line in **c**. AU, arbitrary units. **e**, Periodogram of the *Lfng* oscillations detected in $n = 13$ biologically independent replicates of *LfngT2AVenus* gastruloids, as determined by Lomb–Scargle decomposition (Methods). **f**, Speed of elongation and differentiation front in *LfngT2AVenus* gastruloids treated with PD03 ($n = 14, 9, 10, 9$ and 7 biological replicates for PD03 concentrations $0, 1.3, 13.3, 26.7$ and $66.7 \mu\text{M}$, respectively). In the box plots, centre line indicates median; box limits the 1st and 3rd quartiles; and whiskers the range. Each point is one replicate. A, anterior; P, posterior. Scale bar, $200 \mu\text{m}$.

to recover gene-expression patterns¹² (Fig. 1e, Extended Data Figs. 4, 5, Supplementary Tables 5–8). This comparison revealed a notable similarity between gastruloids and the mesoderm of embryos.

In embryos, the organization of the mesoderm is established by dynamic gene regulatory networks that are tightly linked to the process of somitogenesis⁹. During somitogenesis, retinoic acid and opposing FGF/WNT signalling gradients along the anterior–posterior axis determine the position of the differentiation front, which induces the differentiation of the mesoderm into epithelial blocks known as somites (Fig. 2a). These somites have defined rostral and caudal halves, and appear sequentially in an anterior–posterior direction. During this process, the tail bud of the embryo grows and—consequently—the signalling gradients and differentiation front move posteriorly over time. A second component of somitogenesis entails oscillations of WNT, Notch and FGF signalling, in which signalling waves travel from the tail bud towards the differentiation front about every two hours in mice^{9,13}. This cyclic component of somitogenesis is known as the segmentation clock and is thought to regulate the timing of somite formation^{9,14}. To investigate whether the segmentation clock is active in gastruloids, we monitored Notch signalling activity by performing fluorescence time-lapse imaging on gastruloids generated from *LfngT2AVenus* mouse ES cells¹⁵ (Methods). Similar to what has previously been seen in embryos¹⁵, we observed a dynamic differentiation front that expresses high levels of *Lfng* and regresses posteriorly as the gastruloids extend (Fig. 2b, Extended Data Fig. 7, Supplementary Video 1). Additionally, we observed oscillating waves with low expression of *Lfng* and a period of about 2 h that travel from the tip of the tail bud towards the differentiation front, where they stall (Fig. 2c–e, Extended Data Fig. 8). The expression of *Lfng* disappears in the presence of the Notch inhibitor DAPT (Extended Data Fig. 7e, Supplementary Video 2), which

confirms that the reporter expression is dependent on Notch signalling in gastruloids—as it is in embryos¹⁶. These experiments indicate that the segmentation clock is active in gastruloids with dynamics that are very similar to the in vivo situation.

Gastruloids can easily be generated in large numbers, opening the possibility of performing screens. To exemplify this, we performed a small compound screen on *LfngT2AVenus* gastruloids and investigated the effect of inhibitors and agonists of FGF, WNT and BMP signalling pathways on the speed of the differentiation front (Extended Data Figs. 7, 8e, f, Supplementary Video 3). This revealed that application of the MEK inhibitor PD03—which inhibits FGF signalling—speeds up the differentiation front in a dose-dependent manner, without altering the speed at which gastruloids grow posteriorly (Fig. 2f, Extended Data Fig. 9a, Supplementary Video 4). This imbalance between the speed of the differentiation front and gastruloid growth results in both a progressive decrease in the length of the presomitic mesoderm and in gastruloids that stop growing prematurely (Extended Data Fig. 9b). Similar results were obtained with the FGF-receptor inhibitors PD17 and BGJ398 (Extended Data Figs. 7, 8f, Supplementary Video 5). Our observations provide an explanation for the short-tail phenotype observed in FGF-mutant mouse embryos¹⁷ and for the posteriorly shifted differentiation fronts that have previously been observed after FGF inhibition^{18,19}.

Even though our experiments reveal that key regulators of somitogenesis are expressed in the correct location and that the segmentation clock is active in gastruloids, gastruloids that are generated with previously published protocols do not form somites^{1,3,20}. During our imaging experiments, we occasionally observed small ‘indentations’ that appeared anteriorly to the differentiation front (Supplementary Video 4). These indentations were visible only in gastruloids mounted in Matrigel at 96 h, which was done before the imaging experiments

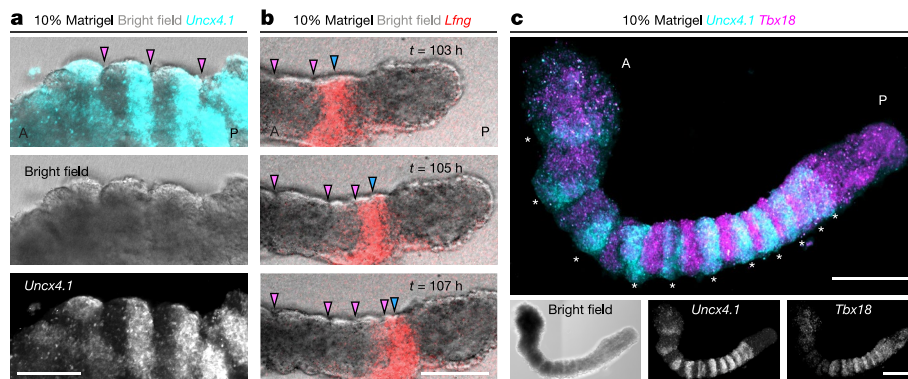


Fig. 3 | Stainings and time-lapse imaging of somite formation in gastruloids embedded in low percentages of Matrigel. **a**, Somites in a representative LfngT2AVenus gastruloid (zoomed in) (Extended Data Fig. 9d) embedded in 10% Matrigel at 96 h and stained for *Uncx4.1* using HCR (ref. ²¹) at 120 h. Magenta arrowheads, segment boundaries. Similar results were obtained in $n = 5$ independent experiments. **b**, Imaging (Supplementary Video 6) of a representative LfngT2AVenus gastruloid embedded in 10% Matrigel at 96 h.

Blue arrowheads, differentiation front (red, *Lfng*-expressing); magenta arrowheads, appearing segment boundaries. Similar results were obtained in $n = 2$ independent experiments. **c**, HCR (ref. ²¹) double staining for *Uncx4.1* (cyan) and *Tbx18* (magenta), on a 120-h LfngT2AVenus gastruloid embedded in 10% Matrigel at 96 h and to which 1.3 μ M of PDO3 was added at 96.5 h. White asterisks, *Uncx4.1* expression stripes. Similar results were obtained in $n = 4$ independent experiments. Scale bars, 100 μ m (**a**, **b**), 200 μ m (**c**).

to stabilize them (Methods). We then performed in situ hybridization stainings for *Uncx4.1* (a marker for the caudal halves of somites⁹) (Fig. 2a) and found that *Uncx4.1* was expressed in a stripy pattern in 4% (4 out of 100) of the 120-h gastruloids that were embedded in 100% Matrigel at 96 h (Extended Data Fig. 9c). This pattern was never detected in 120-h gastruloids cultured without Matrigel. To explore the effect of the concentration of Matrigel, we performed a titration experiment. We found that embedding 96-h gastruloids in 10–25% Matrigel results in the formation of clear segments, of which the posterior half is marked by *Uncx4.1* expression in up to 50% of the gastruloids (in situ hybridization and hybridization chain reaction (HCR)²¹); Fig. 3a, Extended Data Fig. 9c,d). Time-lapse imaging videos of these gastruloids revealed that these segments appear sequentially in an anterior–posterior direction, anteriorly to the *Lfng* expression domain (Fig. 3b, Extended Data Fig. 9e, Supplementary Video 6). Lastly, double stainings for *Uncx4.1* and *Ripply2* (which marks newly forming somites), and for *Uncx4.1* and *Tbx18* (a marker of rostral somites⁹), revealed that *Uncx4.1* and *Tbx18* are expressed in an alternating pattern (Fig. 3c), and that it is indeed the caudal half of the segments that expresses *Uncx4.1* (Extended Data Fig. 10). At 120 h of culture (after 24 h in 10% Matrigel), gastruloids have about 10 or 11 somites (Fig. 3c, Extended Data Fig. 10), the size of which decreases in the anterior–posterior direction from (on average) 183 μ m to 43.4 μ m (Extended Data Fig. 10c–e). In embryos, the size of these somites decreases from 120 μ m to 80 μ m (Methods). Our experiments thus reveal that embedding gastruloids in low-percentage Matrigel induces the formation of somite-like structures, which have the correct rostral–caudal patterning and appear sequentially along the anterior–posterior direction over time. So far, we have not observed gastruloids with two neighbouring rows of somites.

Using single-cell and spatial transcriptomics, we demonstrate that gene expression in mouse gastruloids is very similar to embryos. Gastruloids can therefore be used as a model system for embryology, and have some key advantages over embryos: they can be grown in large quantities (allowing screens), are easier to genetically modify as they can be grown directly from ES cells and can be used to study the effect of external signals on morphogenesis. We used several of these advantages to study somitogenesis in vitro. Recent studies have explored ex vivo and in vitro models for somitogenesis, such as monolayer pre-somitic mesoderm cultures^{16,22} and cultures of embryoid-body-like aggregates of mouse ES cells that display travelling somitogenesis waves in vitro²³. However, such cultures do not form proper somites, lack a correctly defined anterior–posterior axis and do not elongate in

the posterior direction. Here we have shown that gastruloids overcome these limitations, and thus provide a powerful tool for studying somitogenesis in vitro. In general, in vitro mimics of development—such as gastruloids—are promising systems with which we are starting to obtain insights that could not readily be obtained with embryos. We therefore anticipate many applications of this system, which will help to unravel the complex processes that regulate embryogenesis.

Online content

Any methods, additional references, Nature Research reporting summaries, source data, extended data, supplementary information, acknowledgements, peer review information; details of author contributions and competing interests; and statements of data and code availability are available at <https://doi.org/10.1038/s41586-020-2024-3>.

- van den Brink, S. C. et al. Symmetry breaking, germ layer specification and axial organisation in aggregates of mouse embryonic stem cells. *Development* **141**, 4231–4242 (2014).
- Turner, D. A. et al. Anteroposterior polarity and elongation in the absence of extra-embryonic tissues and of spatially localised signalling in gastruloids: mammalian embryonic organoids. *Development* **144**, 3894–3906 (2017).
- Beccari, L. et al. Multi-axial self-organization properties of mouse embryonic stem cells into gastruloids. *Nature* **562**, 272–276 (2018).
- Pijuan-Sala, B. et al. A single-cell molecular map of mouse gastrulation and early organogenesis. *Nature* **566**, 490–495 (2019).
- Nowotschin, S. et al. The emergent landscape of the mouse gut endoderm at single-cell resolution. *Nature* **569**, 361–367 (2019).
- Kwon, G. S., Viotti, M. & Hadjantonakis, A. K. The endoderm of the mouse embryo arises by dynamic widespread intercalation of embryonic and extraembryonic lineages. *Dev. Cell* **15**, 509–520 (2008).
- Scotti, M. & Kmita, M. Recruitment of 5' Hoxa genes in the allantois is essential for proper extra-embryonic function in placental mammals. *Development* **139**, 731–739 (2012).
- Koch, F. et al. Antagonistic activities of Sox2 and *Brachyury* control the fate choice of neuro-mesodermal progenitors. *Dev. Cell* **42**, 514–526 (2017).
- Chal, J. & Pourquié, O. Making muscle: skeletal myogenesis in vivo and in vitro. *Development* **144**, 2104–2122 (2017).
- Laurent, F. et al. HAND2 target gene regulatory networks control atrioventricular canal and cardiac valve development. *Cell Rep.* **19**, 1602–1613 (2017).
- Junker, J. P. et al. Genome-wide RNA tomography in the zebrafish embryo. *Cell* **159**, 662–675 (2014).
- Chal, J. et al. Differentiation of pluripotent stem cells to muscle fiber to model Duchenne muscular dystrophy. *Nat. Biotechnol.* **33**, 962–969 (2015).
- Dequéant, M. L. et al. A complex oscillating network of signaling genes underlies the mouse segmentation clock. *Science* **314**, 1595–1598 (2006).
- Oates, A. C., Morelli, L. G. & Ares, S. Patterning embryos with oscillations: structure, function and dynamics of the vertebrate segmentation clock. *Development* **139**, 625–639 (2012).
- Sonnen, K. F. et al. Modulation of phase shift between Wnt and Notch signaling oscillations controls mesoderm segmentation. *Cell* **172**, 1079–1090.e12 (2018).

16. Hubaud, A., Regev, I., Mahadevan, L. & Pourquié, O. Excitable dynamics and Yap-dependent mechanical cues drive the segmentation clock. *Cell* **171**, 668–682.e11 (2017).
17. Naiche, L. A., Holder, N. & Lewandoski, M. FGF4 and FGF8 comprise the wavefront activity that controls somitogenesis. *Proc. Natl Acad. Sci. USA* **108**, 4018–4023 (2011).
18. Dubrulle, J., McGrew, M. J. & Pourquié, O. FGF signaling controls somite boundary position and regulates segmentation clock control of spatiotemporal Hox gene activation. *Cell* **106**, 219–232 (2001).
19. Sawada, A. et al. Fgf/MAPK signalling is a crucial positional cue in somite boundary formation. *Development* **128**, 4873–4880 (2001).
20. Baillie-Johnson, P., van den Brink, S. C., Balayo, T., Turner, D. A. & Martinez Arias, A. Generation of aggregates of mouse embryonic stem cells that show symmetry breaking, polarization and emergent collective behaviour in vitro. *J. Vis. Exp.* **105**, e53252 (2015).
21. Choi, H. M. T. et al. Third-generation *in situ* hybridization chain reaction: multiplexed, quantitative, sensitive, versatile, robust. *Development* **145**, dev165753 (2018).
22. Lauschke, V. M., Tsiairis, C. D., François, P. & Aulehla, A. Scaling of embryonic patterning based on phase-gradient encoding. *Nature* **493**, 101–105 (2013).
23. Matsumiya, M., Tomita, T., Yoshioka-Kobayashi, K., Isomura, A. & Kageyama, R. ES cell-derived presomitic mesoderm-like tissues for analysis of synchronized oscillations in the segmentation clock. *Development* **145**, dev156836 (2018).

Publisher's note Springer Nature remains neutral with regard to jurisdictional claims in published maps and institutional affiliations.

© The Author(s), under exclusive licence to Springer Nature Limited 2020

Methods

Mouse gastruloid culture, with and without Matrigel

E14-IB10 (a subclone of 129/Ola-derived E14 ES cells, from The Netherlands Cancer Institute), LfngT2AVenus¹⁵ (Notch signalling reporter, which contains a single copy of Venus that was inserted in the endogenous *Lfng* locus¹⁵; the selection cassette was removed), *Brachyury-GFP* (ref. ²⁴), WNT/ β -catenin transcriptional reporter TCF/LEF-*mCherry* (refs. ^{25,26}) and *Nodal-YFP* (ref. ²⁷) mouse ES cells were maintained in standard conditions in ESLIF medium (GMEM supplemented with sodium pyruvate, non-essential amino acids, GlutaMAX, penicillin–streptomycin, β -mercaptoethanol, 10% FBS and LIF) on gelatinized 6-well plates and in a humidified incubator (5% CO₂, 37 °C) as previously described^{20,25,28–31} (Supplementary Methods 1, 2). E14-IB10 mouse ES cells were obtained from E. R. Maandag (Netherlands Cancer Institute). LfngT2AVenus mouse ES cells from which the selection cassette has been removed were obtained from the Aulehla laboratory. *Brachyury-GFP* mouse ES cells were obtained from the Keller laboratory. TCF/LEF-*mCherry* mouse ES cells were obtained from the Hadjantonakis laboratory, and *Nodal-YFP* mouse ES cells were obtained from the Collington laboratory. These cell lines were validated as follows: for the *Brachyury-GFP* and TCF/LEF-*mCherry* lines, stimulation with Chiron resulted in reporter expression in a region that overlapped with the expression of *Brachyury* or *Wnt3a*, respectively, in our tomo-seq data (Extended Data Fig. 3d); for the *Nodal-YFP* line, we tested whether the reporter expression was blocked by the Nodal inhibitor SB43 and switched on by Nodal and activin A; for the LfngT2AVenus line, we showed dynamics very similar to the dynamics reported in embryos in vivo, and tested whether the reporter signal disappeared upon application of the Notch inhibitor DAPT. Our RNA sequencing experiments confirmed that all these cell lines were derived from mice. All cell lines were routinely tested and confirmed to be free of mycoplasma.

Gastruloids for scRNA-seq and tomo-seq experiments were generated as previously described^{1,20}, with the following minor modifications: after neutralization of trypsin with ESLIF, cells were washed with PBS (containing Ca²⁺ and Mg²⁺) twice. Next, cells were resuspended in N2B27 medium (NDiff227 medium, Takara, Y40002), and the cell concentration was determined only after resuspension in N2B27 medium. Cells were then diluted in N2B27 to a concentration of 7.5 cells per microlitre, and 40 μ l (with about 300 cells) of this suspension was transferred to each well of a U-bottomed 96-well plate (Greiner Bio-One, 650185). N2B27 aliquots were stored at –20 °C and thawed by rocking them at 4 °C for several hours, after which aliquots were transferred to a cell-culture flask in a CO₂-controlled 37-°C incubator for pH equilibration 1 day before gastruloid formation. A step-by-step protocol is provided in the Supplementary Methods. Aggregates that did not elongate and that did not form gastruloids were excluded from this study, and curved gastruloids were excluded from tomo-seq experiments. For the scRNA-seq and tomo-seq experiments, 120-h gastruloids generated with the original gastruloids protocol^{1,20} were used, as these gastruloids were—in our experiments—more reproducible (showing considerably less variation in morphology between wells) than more recent versions of the protocol that allow culture up to 168 h (ref. ³). For in situ hybridization, HCR staining and imaging experiments, gastruloids were cultured as described, but then embedded in Matrigel at 96 h. To embed gastruloids in 50–100% Matrigel (Corning, 356231, lot number 6137007, protein concentration 9.8 mg/ml), Matrigel was thawed on ice, mixed with the required amount of cold N2B27 medium and 60 μ l was added to each well of a multiwell imaging chamber (Sigma, EP0030741021 or M9312) on ice. Ninety-six-hour gastruloids were then transferred to the Matrigel using a 20- μ l pipette and allowed to settle for approximately 5 min before the chamber was incubated at 37 °C for 10 min, allowing the Matrigel to solidify. After this, 500 μ l N2B27 medium was added to each well. Embedding gastruloids in diluted 10–25% Matrigel was done by first pooling the gastruloids in a 5-ml DNA LoBind Eppendorf

tube on ice, replacing the N2B27 medium with fresh cold medium and then adding the correct volume of Matrigel. The gastruloids were then transferred to a 24-well plate (Sigma, EP0030741021 or M9312) using a P1000 pipette with the tip cut off, at a concentration of about 8 gastruloids per ml, 500 μ l per well; plates were gently agitated to prevent gastruloids from clumping together in the centre of the wells before the plates were placed in the incubator. In our experiments, somite formation was more efficient when gastruloids were generated from cells with a low passage number. In all experiments, gastruloids were allocated to the various conditions randomly. No statistical methods were used to predetermine sample size, and blinding was not relevant to the study. A step-by-step protocol describing how gastruloids were cultured, embedded in Matrigel and fixed is provided in the Supplementary Methods. This protocol has also been deposited in the Protocol Exchange repository³².

Dissociation and fluorescence-activated cell sorting of gastruloids before scRNA-seq

To dissociate gastruloids for scRNA-seq, gastruloids were washed with PBS twice, incubated in trypsin–EDTA at 37 °C for 5 min and titrated with a P200 pipette, after which ESLIF was added to neutralize the trypsin. After centrifugation (200g, 3 min), cells were resuspended in PBS with 10% serum and filtered through a 35- μ m filter (Falcon, 352235). Prior to fluorescence-activated cell sorting (FACS), DAPI (Thermo Fisher) was added to assess cell viability. For SORT-seq, individual live cells were sorted into the wells of a 384-well plate as previously described³³ using a BD FACSJazz Cell Sorter (BD Biosciences) that was equipped with BD FACS software (version 1.2.0.124). For 10x Genomics scRNA-seq, washes were done using PBS0 (PBS without calcium and magnesium), and 100,000 live cells were sorted into 1.5-ml DNA LoBind tubes (Eppendorf, 022431021) that were pre-filled with 50 μ l PBS0, after which cells were centrifuged for 3 min at 200g, resuspended in 80 μ l PBS0 containing 5–10% serum, and filtered through a 35- μ m filter (Falcon, 352235). After resuspension and filtering, the cell concentration was determined using a counting chamber (Bürker-Türk, Marienfeld).

SORT-seq and 10x Genomics scRNA-seq

For scRNA-seq, cells extracted from 120-h gastruloids (generated with a previously published, non-Matrigel-based protocol^{1,20}) were processed using either SORT-seq (CEL-seq2-based scRNA-seq on cells that were sorted into 384-well plates³³) or using the 10x Genomics Chromium Single Cell 3' (v.3 Chemistry) gene-expression kit, according to manufacturer's instructions.

Mouse experimentation

Mouse embryos ($n = 3$) used for tomo-seq were derived from crosses between CD-1 females and CD-1 stud males. Experiments were performed in accordance with European Union (EU) guidelines, under the authority of appropriate UK governmental legislation. All mouse experiments for this project were approved by the Animal Welfare and Ethical Review Body for the University of Cambridge. Relevant Home Office licences are in place.

Tomo-seq

Tomo-seq was performed using a robotized (SORT-seq³³-based) version of a previously published tomo-seq protocol¹¹. In brief, 120-h gastruloids ($n = 3$ E14-IB10 gastruloids sectioned along their anterior–posterior axis using 20- μ m sections; $n = 2$ E14-IB10 gastruloids sectioned along their anterior–posterior axis using 8- μ m sections; and $n = 3$ LfngT2AVenus gastruloids sectioned along their anterior–posterior axis using 20- μ m sections, generated with previously published, non-Matrigel-based gastruloid protocols^{1,20}) or E8.5 mouse embryos ($n = 3$ sectioned along their anterior–posterior axis using 20- μ m sections) were embedded in cryosolution (Leica, 14020108926), snap-frozen on dry ice, stored at –80 °C and sectioned using a cryotome. Sections were collected in the

wells of a hard-shell PCR low-profile, semi-skirted 96-well plate (Bio-rad, HSL9601) that was prefilled with mineral oil (Sigma, M8410-1L) and CEL-seq2 primers. For each well, a unique, barcoded CEL-seq2 primer was used, which allowed us to pool the content of the wells after second-strand synthesis. To sequence the mRNA content of the wells, SORT-seq (robotized CEL-seq2-based scRNA-seq³³) was performed using a Nanodrop II liquid handling platform (GC biotech).

Sequencing

Sequencing was performed on the Illumina next-seq sequencing platform. For SORT-seq and tomo-seq, paired-end (75-bp) sequencing was performed; and for 10x Genomics, sequencing was performed according to 10x Genomics manufacturer's instructions (read 1, 28 cycles; index i7, 8 cycles; and read 2, 91 cycles).

Mapping sequencing data

For SORT-seq and tomo-seq, the first six bases of read 1 contain the unique molecular identifier and the next seven bases contain the cell or section barcode. For 10x Genomics, the first 16 bases of read 1 contain the cell barcode, and the next 12 contain the unique molecular identifier. For all sequencing experiments, read 2 contains the biological information. Reads 2 with a valid cell or section barcode were selected, trimmed using TrimGalore (v.0.4.3) with default parameters, and mapped using STAR (v.2.5.3a) with default parameters to the mouse mm10 genome (Ensembl 93). Only reads mapping to gene bodies (exons or introns) were used for downstream analysis. Reads mapping simultaneously to an exon and to an intron were assigned to the exon. For each cell or section, the number of transcripts was obtained as previously described³⁴. We refer to transcripts as unique molecules based on unique molecular identifier correction. Mappabilities for both scRNA-seq and tomo-seq experiments range from 35% to 60%. Spike-ins, ribosomal and mitochondrial genes were removed from downstream analysis, together with *Kcnq1ot1*, *Lars2* and *Malat1*, because these genes seem to be linked to mapping errors and have previously been shown to be erroneous³⁴.

Processing single-cell data

scRNA-seq analysis was performed using the Scanpy package³⁵ (v.1.4.3). In each experiment, cell barcodes with more than 1,000 transcripts and fewer than 6,000 genes were selected. Genes detected in fewer than three cells were excluded. Expression levels for each cell were size-normalized to 10,000 transcripts. Highly variable genes were defined as those with a mean expression value between 0.0125 and 5, and with a minimum dispersion, and used to generate the UMAP plots shown in Fig. 1, Extended Data Figs. 1, 2, 4, 5. Next, cells from the three independent experiments were analysed together. Here, we kept cells with more than 700 and fewer than 8,000 genes, and more than 1,000 and fewer than 40,000 transcripts. Selection of highly variable genes and cell normalization were then performed. To remove batch effects, we used the combat function from Scanpy (a Python implementation (<https://github.com/brentp/combat.py>) of the R- package Bioconductor^{36,37}). Cells were clustered using a combination of *k*-medoids and Leiden algorithms³⁸ (Supplementary Table 1). Differentially expressed genes in each cluster were determined using the *t*-test (Supplementary Table 2).

Comparison between gastruloid cell types and mouse embryonic-cell types

Common genes between marker genes detected in the gastruloid cell clusters (Supplementary Table 1) (P value < 0.01 and \log_2 -transformed fold change > 1.01) and marker genes found for the different embryonic-cell types defined in a previously published mouse embryo scRNA-seq dataset⁴ were found. P value for significance was assigned using a binomial test, in which the probability of sharing a number of common marker genes between a gastruloid cell type and an embryonic-cell type was determined by randomizing the list of marker genes for the embryonic-cell type from the full list of marker genes in the embryonic-cell

types ($n = 200$). Extended Data Fig. 1h shows only the comparison to embryonic-cell types found at E8.5. Extended Data Fig. 1i shows the comparison to all embryonic-cell types detected from E7.0 until E8.5. Only embryonic cell types with at least one cluster comparison with a P value below 0.2 are shown. Using different P value thresholds to define upregulated genes does not have a considerable effect on the results of the comparison between gastruloid cell populations and embryonic cell types.

Linearization of the UMAP plot

Cells in clusters 1–8 were projected on the symmetry axis along the clusters 1–8 in the UMAP plot (Extended Data Fig. 1d). The position of each cell along this symmetry axis defines the x -position in Extended Data Fig. 2d. To plot gene expression along the linearized UMAP plot, 1,000 evenly spaced bins were defined along the x -axis for which the expression average of all cells per respective bin was scaled and plotted. For visualization, a LOESS smoother was used with span set to 0.2.

Processing tomo-seq data

Twenty-micrometre sectioned slices with fewer than 3,200 genes and 8- μ m sectioned slices with fewer than 6,000 genes were filtered out (Extended Data Fig. 3). In each tomo-seq sample, data were normalized to the median number of unique transcripts per slide. Sequencing libraries contain a maximum of 96 slices. In samples with more than 96 sections, several libraries were generated. For these samples, we corrected batch effects between sequenced libraries by imposing the continuity of expression profiles along the anterior–posterior axis for each gene separately.

Gene reproducibility analysis between replicates

The Pearson correlation coefficient between the anterior–posterior expression pattern (in z -score units) of two different samples is computed for all possible pairs of replicates. Linearly interpolated gene-expression profiles are used when the number of sections is different between replicates. To assess for significant correlations, we randomly generate 10,000 expression profiles with the same number of sections as in the pair of replicates and determine a threshold for the correlation value at which less than n random profiles have larger correlation values ($n = 100$ for P value < 0.01, $n = 500$ for P value < 0.05 and so on) (Supplementary Table 5). Adjusted P values are obtained with the Benjamini–Hochberg correction. Only genes that are significantly correlated (P value < 0.01) in at least five possible pairs of replicates are considered as reproducible between replicates (Supplementary Tables 6, 9). Custom-made code was used for this analysis.

Clustering genes on the basis of anterior–posterior expression patterns

Genes were first clustered on the basis of z -score anterior–posterior expression pattern using self-organizing maps with an initial number of clusters set to about $5\sqrt{n}$, in which n is the total number of genes. Average z -score expression patterns for each cluster were then hierarchically clustered using Euclidean distances and the Ward.D method.

Comparison between tomo-seq data of mouse embryos, mouse gastruloids and mouse presomitic mesoderm dataset

Gene reproducibility analyses between the individual replicates of the systems that are being compared were performed independently, as described in 'Gene reproducibility analysis between replicates' (Supplementary Tables 5–9). For heat maps in Fig. 1b, d, e, only genes present in the two separate lists of significantly correlated genes were used for downstream analysis (Supplementary Tables 7, 9). For heat maps in Extended Data Fig. 5, genes that were present in only one of the two separate lists were included as well (Supplementary Tables 8, 9). Genes were clustered on the basis of their anterior–posterior expression pattern in the systems that were being compared simultaneously, as

Article

described in 'Clustering genes on the basis of anterior-posterior expression patterns'. The Pearson correlation coefficient for each gene was calculated between the anterior–posterior expression pattern of two different samples (in z-score units). To assess for significantly correlated genes, we randomly generated 10,000 expression profiles with the same number of sections as in the pair of replicates and determined the correlation value at which less than 500 random profiles have larger correlation values (P value < 0.05). Adjusted P values were obtained with the Benjamini–Hochberg correction. For the presomitic mesoderm comparison, we used a previously published microarray dataset in which the posterior mesoderm (from the tail bud to the newly formed somite) of E9.5 mouse embryos was investigated¹² (accession number GSE39615).

Comparison between genes in tomo-seq clusters and mouse embryonic-cell types

This was performed as described in 'Comparison between gastruloid cell types and mouse embryonic-cell types', but then calculating the number of overlapping genes and the P value of this overlap by comparing the genes in each tomo-seq cluster with the list of genes upregulated in the cell types of a previously published E8.5 mouse embryo scRNA-seq dataset⁴ (Supplementary Tables 5–9).

Wide-field microscopy

Wide-field images of gastruloids made from *Brachyury-GFP* (ref. ²⁴), *Nodal-YFP* (ref. ²⁷) and *TCF/LEF-mCherry* (TLC2) (refs. ^{25,26}) mouse ES cells were acquired at 120 h using a Zeiss AxioObserver Z1 in a humidified CO₂ incubator (5% CO₂, 37 °C) and a 20× LD Plan-Neofluar 0.4 NA Ph2 objective with the correction collar set to image through plastic, as previously described². Illumination was provided by an LED white-light system (Laser2000) in combination with filter cubes GFP-1828A-ZHE (Semrock), YFP-2427B-ZHE (Semrock) and Filter Set 45 (Carl Zeiss Microscopy) used for GFP, YFP and RFP, respectively. Emitted light was recorded using a back-illuminated iXon888 Ultra EMCCD (Andor) and images were processed using Fiji (v.2.0.0)³⁹.

Multiphoton time-lapse imaging of gastruloids

Gastruloids were embedded in 10–100% Matrigel in 24-well plates (Sigma, EPO030741021 or M9312) at 96 h as described in 'Mouse gastruloid culture, with and without Matrigel' (Supplementary Methods 3), and imaged immediately following embedding at 37 °C, 5% CO₂ with humidified air influx on a Leica SP8 multiphoton microscope system using an HC PL APO 20×/0.75 air CS2 objective, a Coherent Chameleon Vision-S multiphoton laser tuned to 960 nm and the pinhole maximally opened. The bright field channel was recorded using a 488-nm laser set at low intensity in combination with a transmission PMT. A z-stack of around 4 images with a z-interval of 15 μm was taken every 15 min (10 images per stack and at 12 min interval) (Fig. 3b) for each individual gastruloid (frame accumulation 2 times, pixel dwell time 2.425 μs). Photons with a wavelength between 505–555 nm, and 555–680 nm were collected with two separate hybrid detectors and assigned to a 16-bit pixel range. Alternatively, in Extended Data Fig. 7d, a 514-nm solid state laser was used, during which photons were collected with a wavelength between 524–575 nm and 600–700 nm with two separate hybrid detectors and assigned to a 16-bit pixel range. In this case, the bright field channel was recorded simultaneously with the other channels using a transmission photomultiplier tube.

Treatment of Matrigel-embedded gastruloids with inhibitors

Gastruloids were embedded in 10–100% Matrigel at 96 h as described in 'Mouse gastruloid culture, with and without Matrigel', and time-lapse imaging was started immediately after embedding. After recording at least 2 time points (and at most 4 time points) for each replicate (about 30–60 min in total), the microscope was paused and inhibitors were added without removing the culturing plate from the stage.

The inhibitors used were DAPT (Sigma, D5942; stock 10 mM in DMSO; used at 27 μM); PD0325901 (Sigma, PZ0162; stock 10 mM in DMSO); BJJ398 (Selleckchem, S2183; stock 1 mM in DMSO; used at 0.2 μM); PD173074 (Peprotech, 2191178; stock 10 mM in DMSO; used at 0.5 μM); FGF1 (Peprotech, 100-17A; stock 10 μg/ml in H₂O; used at 0.02 μg/ml); FGF10 (Peprotech, 100-26; stock 100 μg/ml in H₂O; used at 0.2 μg/ml); Chiron (CHI99021; Sigma, SML1046; stock 10 mM in DMSO; used at 10 μM); IWP-2 (Sigma, I0536; stock 2 mM in DMSO; used at 2 μM); IWR-1 (Sigma, I0161; stock 10 mM in DMSO; used at 10 μM); and LDN193189 (Sigma, SML0559; stock 0.1 mM in H₂O; used at 0.2 μM).

Analysis of multiphoton time-lapse imaging data

Image analysis was done similarly to previously described image-analysis methods^{15,22}. Time-lapse imaging data were analysed using the ImageJ data processing package Fiji (v.2.0.0)³⁹. To filter out autofluorescence, the first channel (555–680 nm) was multiplied by 0.3 and subtracted from the second channel (505–555 nm). Then, a sum projection of all z-slices was generated for all time points. The resulting image was convolved using a Gaussian filter with a sigma value of 1 μm. Kymographs were generated using the plug-in KymoResliceWide (v.0.5, <https://github.com/ekatrakha/KymoResliceWide>) by tracing the path of the differentiation front as it moves along the anterior–posterior axis with a segmented line (60 pixels wide) and then blurred using a Gaussian filter with a sigma value of 1 pixel. The intensity profile of the oscillations was measured at a constant distance from the differentiation front (dashed white line in Fig. 2c) on the kymograph. The intensity profile of the oscillations was decomposed into a trend and a cycle component using Hodrick–Prescott filtering with an l of 800. Trend and cycle components for all replicates are shown in Extended Data Fig. 8. To make an estimation of the period of the *Lfng* oscillations, Lomb–Scargle analysis was performed with the maximum scanned frequency at half the temporal resolution and over-sampling set to 3 (ref. ⁴⁰). The speed of the differentiation front and the elongation speed of the gastruloid were measured by first drawing a line along the differentiation front or posterior tip of the gastruloid on the kymograph, respectively, and then measuring the angle, as explained in Extended Data Fig. 9a.

Sample fixation for staining

For gastruloids grown in 100–50% Matrigel, the medium was removed and the samples were washed twice for 5 min in PBS before fixation in 4% PFA in PBS overnight at 4 °C. For gastruloids grown in 25–10% Matrigel, the Matrigel was not removed in the first washing step with PBS (Supplementary Methods 4). After fixation, all samples were washed 3 times for 5 min in PBS-Tween (0.1% Tween-20 (v/v)), transferred to DNA LoBind tubes using a P1000 pipette with the tip cut off, and washed 3 times for 3 min in TBS-Tween (0.1% Tween-20 (v/v)) before digesting for 4 min with 25 μg/ml proteinase K in TBS-Tween. The samples were then rinsed briefly 3 times with 2 mg/ml glycine in TBS-Tween20, washed with TBS-Tween once, refixed for 30 min in 4% PFA and 0.05% GA in PBS at room temperature and washed 3 times in TBS-Tween.

In situ hybridization

In situ hybridization was performed as previously described^{3,15}. In brief, samples were incubated for 4–5 h in hybridization mix (5 mg/ml torula RNA (Sigma, R6625), 50% deionized formamide (Sigma, AM9342) (v/v), 1.33x SSC, 0.1% BSA (w/v), 125 μg/ml heparin (Sigma, H3393), 10 mM EDTA 0.5 pH = 8.0, 0.1% Tween 20 (v/v)) at 68 °C followed by incubation overnight in 150 ng/ml DIG-labelled probe in hybridization mix at 68 °C. Carryover Matrigel that was still present degraded during this incubation step in most instances. The hybridization mix with the probe was preincubated for 10 min at 80 °C. Samples were then washed twice for 30 min in preheated hybridization mix at 68 °C, 4 times for 20 min in preheated 2x SSC-Tween (0.1% Tween-20 (v/v)) at 68 °C, allowed to cool down and washed twice for 5 min in MAB-Tween (0.1% Tween-20 (v/v)) at room temperature. The samples were blocked for 1.5 h in blocking

buffer (10% heat-inactivated sheep serum (Sigma, S3772) (v/v) and 1% BSA (w/v) in MAB-Tween) at room temperature, incubated for 4–5 h in blocking buffer containing 1:2,000 anti-DIG-AP antibody (Sigma, I1093274910) at room temperature and washed 5 times for 10 min followed by washing overnight in MAB-Tween. Finally, the samples were washed 3 times in TBS-Tween, washed 3 times for 10 min in AP-buffer (100 mM Tris-HCl pH 8.0, 100 mM NaCl, 50 mM MgCl₂, 0.1% Tween-20), stained for several hours in 1 ml BM purple (Sigma, I1442074001), washed 3 times for 5 min in TBS-Tween and refixed in 4% PFA/PBS for 20 min at room temperature.

Imaging of gastruloids stained with in situ hybridization

In situ samples were imaged on a Leica M165FC stereo microscope with DMC5400 digital camera (Extended Data Fig. 9c, right) or using a Nikon SMZ800N microscope (Extended Data Fig. 9c, left panels) in TBS-Tween.

HCR of 10% Matrigel-embedded gastruloids

In situ whole mount HCR V3 was performed as previously described²¹ using reagents from Molecular Instruments. In brief, each condition (up to 100 gastruloids) was incubated in 200–500 µl of probe hybridization buffer for 5 min at room temperature and 30 min at 37 °C before incubation with 4 pM of each probe stock in 200–500 µl probe hybridization buffer for 12–16 h at 37 °C. Next, samples were washed 4× with 500 µl probe wash buffer for 15 min at 37 °C, 2× with 1 ml 5× SSC-Tween for 10 min at room temperature and 1× with 200–500 µl amplification buffer for 5 min at room temperature. The hairpin mixture was prepared by separately heating both h1 and h2 of each hairpin to 95 °C for 90 s and incubating these at room temperature for 30 min in the dark. All the hairpin mixtures were then added to 200–500 µl amplification buffer at a concentration of 48 pM, which was then added to the samples and incubated for 12–16 h at room temperature in the dark. Samples were then washed at least 2× with 1 ml SSC-Tween for 30 min before imaging. HCR probe design was as follows: *Uncx4.1* (Accession NM_013702.3, hairpin B1); *Tbx18* (Accession NM_023814.4, hairpin B3); *Ripply2* (Accession NM_001037907, hairpin B2); hairpin B1 was labelled with Alexa 594 and B2 and B3 with Alexa 488.

Multiphoton microscopy of HCR-stained gastruloids

HCR-stained samples were imaged in TBS-T on a Leica SP8 multiphoton microscope system using an HC PL APO 20×/0.75 air CS2 objective, a Coherent Chameleon Vision-S multiphoton laser tuned to 810 nm for the Alexa-594 dye, a 488-nm OPS-laser for the Alexa-488 dye and the pinhole maximally opened. A z-stack of around 30 images with a z-interval of 5 µm was taken with frame accumulation set to 4. Photons with a wavelength between 505–555 nm and 555–680 nm were collected with two separate hybrid detectors and assigned to a 16-bit pixel range for the Alexa-594 channel; photons with a wavelength between 498 and 550 nm were collected with a hybrid detector and assigned to a 16-bit pixel range for the Alexa-488 channel. The bright field channel was recorded simultaneously with the Alexa-488 channel using a transmission photomultiplier tube detector.

HCR data analysis

HCR imaging data were analysed using the ImageJ data processing package Fiji (v.2.0.0)³⁹. First, all the images in a single stack were aligned using the ImageJ plug-in Correlescence (v.0.0.3, <https://github.com/ekatrakha/Correlescence>), after which a maximum projection was generated for the fluorescence channels. The posterior region of gastruloids was identified visually (the anterior end of gastruloids is darker than the posterior end), and confirmed with *Ripply2* staining. To plot the intensity profile along the anterior–posterior axis, a segmented line with a width of 100 pixels was drawn, and the intensity was measured along this line. To measure the peak-to-peak distances in the *Uncx4.1* intensity profiles, a LOWESS smoother (0.002 span) was applied, after

which the maximal values corresponding to the peaks were selected in R (v.3.6.1).

Somite-size measurements in embryos

Somite sizes were measured in 10 somite-stage paraffin-embedded mouse embryos that were sectioned with 6-µm sections, stained using a standard haematoxylin and eosin staining and imaged with a Leica DM 4000 B LED microscope with Leica DFC450 camera that was size-calibrated using a microscope calibration slide (Pyser-SGI). Somite sizes were next measured using Fiji (v.2.0.0). Measurements were validated by comparing results to somite sizes in the EMAP eMouse Atlas Project (<http://www.emouseatlas.org>)⁴¹.

Reporting summary

Further information on research design is available in the Nature Research Reporting Summary linked to this paper.

Data availability

All RNA sequencing datasets produced in this study are deposited in the Gene Expression Omnibus (GEO) under accession code GSE123187. All scRNA-seq and tomo-seq data can be explored at <https://avolab.hubrecht.eu/MouseGastruloids2020>. Source Data for Figs. 1, 2 and Extended Data Fig. 1–6, 8, 10 are provided with the paper. Any other relevant data are available from the corresponding authors upon reasonable request.

Code availability

All code is available at https://github.com/anna-alemany/mouseGastruloids_scRNAseq_tomoseq and <https://github.com/vincentvatenburg/MouseGastruloids>.

- Fehling, H. J. et al. Tracking mesoderm induction and its specification to the hemangioblast during embryonic stem cell differentiation. *Development* **130**, 4217–4227 (2003).
- Faunes, F. et al. A membrane-associated β-catenin/Oct4 complex correlates with ground-state pluripotency in mouse embryonic stem cells. *Development* **140**, 1171–1183 (2013).
- Ferrer-Vaquero, A. et al. A sensitive and bright single-cell resolution live imaging reporter of Wnt/β-catenin signaling in the mouse. *BMC Dev. Biol.* **10**, 121 (2010).
- Papanayotou, C. et al. A novel *Nodal* enhancer dependent on pluripotency factors and Smad2/3 signaling conditions a regulatory switch during epiblast maturation. *PLoS Biol.* **12**, e1001890 (2014).
- Kalmar, T. et al. Regulated fluctuations in Nanog expression mediate cell fate decisions in embryonic stem cells. *PLoS Biol.* **7**, e1000149 (2009).
- Turner, D. A. et al. Wnt/β-catenin and FGF signalling direct the specification and maintenance of a neuroepidermal axial progenitor in ensembles of mouse embryonic stem cells. *Development* **141**, 4243–4253 (2014).
- Turner, D. A., Rué, P., Mackenzie, J. P., Davies, E. & Martinez Arias, A. Brachyury cooperates with Wnt/β-catenin signalling to elicit primitive-streak-like behaviour in differentiating mouse embryonic stem cells. *BMC Biol.* **12**, 63 (2014).
- Turner, D. A., Trott, J., Hayward, P., Rué, P. & Martinez Arias, A. An interplay between extracellular signalling and the dynamics of the exit from pluripotency drives cell fate decisions in mouse ES cells. *Biol. Open* **3**, 614–626 (2014).
- van Batenburg, V. et al. Generating gastruloids with somite-like structures from mouse embryonic stem cells. *Protoc. Exch.* <https://doi.org/10.21203/rs.2.18203/v1> (2020).
- Muraro, M. J. et al. A single-cell transcriptome atlas of the human pancreas. *Cell Syst.* **3**, 385–394.e3 (2016).
- Grün, D. et al. Single-cell messenger RNA sequencing reveals rare intestinal cell types. *Nature* **525**, 251–255 (2015).
- Wolf, F. A., Angerer, P. & Theis, F. J. SCANPY: large-scale single-cell gene expression data analysis. *Genome Biol.* **19**, 15 (2018).
- Johnson, W. E., Li, C. & Rabinovic, A. Adjusting batch effects in microarray expression data using empirical Bayes methods. *Biostatistics* **8**, 118–127 (2007).
- Chakraborty, S., Datta, S. & Datta, S. Surrogate variable analysis using partial least squares (SVA-PLS) in gene expression studies. *Bioinformatics* **28**, 799–806 (2012).
- Traag, V. A., Waltman, L. & van Eck, N. J. From Louvain to Leiden: guaranteeing well-connected communities. *Sci. Rep.* **9**, 5233 (2019).
- Schindelin, J. et al. Fiji: an open-source platform for biological-image analysis. *Nat. Methods* **9**, 676–682 (2012).
- Glynn, E. F., Chen, J. & Mushegian, A. R. Detecting periodic patterns in unevenly spaced gene expression time series using Lomb–Scargle periodograms. *Bioinformatics* **22**, 310–316 (2006).
- Richardson, L. et al. EMAGE mouse embryo spatial gene expression database: 2014 update. *Nucleic Acids Res.* **42**, D835–D844 (2014).
- van den Brink, S. C. et al. Single-cell sequencing reveals dissociation-induced gene expression in tissue subpopulations. *Nat. Methods* **14**, 935–936 (2017).

Article

Acknowledgements This work was supported by an European Research Council Advanced grant (ERC-AdG 742225-IntScOmics), a Nederlandse Organisatie voor Wetenschappelijk Onderzoek (NWO) TOP award (NWO-CW 714.016.001) and the Foundation for Fundamental Research on Matter, financially supported by NWO (FOM-14NOISE01) to S.C.v.d.B., A.A., V.v.B., M.B., J.V. and A.v.O., a Biotechnology and Biological Sciences Research Council (no. BB/P003184/1), Newton Trust (INT16.24b) and Medical Research Council (MR/R017190/1) grant to A.M.A., a Newnham College Cambridge Junior Research Fellowship to N.M. and a studentship from the Engineering and Physical Sciences Research Council to P.B.-J. The Cambridge Stem Cell Institute is supported by core funding from the Wellcome Trust and Medical Research Council; J.N. was funded by the University of Cambridge and K.F.S. by core funding from the Hubrecht Institute. This work is part of the Oncode Institute, which is partly financed by the Dutch Cancer Society. We thank A. Ebbing and M. Betist for the robotized tomo-seq protocol; G. Keller for the *Brachyury-GFP* cell line; J. Collignon for the *Nodal-YFP* line; K. Hadjantonakis for the *TCF/LEF-mCherry* line; S. van den Brink and E. R. Maandag for the E14-IB10 cells; J. Kress and A. Aulehla for the *LfngT2AVenus* mouse ES cell line; I. Misteli Guerreiro, J. Peterson-Maduro and J. Hoeksma for suggestions for in situ hybridization experiments; W. Thomas, Y. el Azhar, J. Juksar and J. Beumer for reagents and inhibitors; A. de Graaff and A. Stokkermans for help with multiphoton microscopy and analysis of the microscopy data; D. A. Turner for microscopy panels that were used for tomo-seq validation; J. Korving for help with the somite-size measurements in embryos; the Hubrecht FACS facility and R. van der Linden for FACS experiments; Single Cell Discoveries for 10x Genomics scRNA-seq; the Utrecht Sequencing facility for sequencing; and P. Zeller, H. Viñas Gaza, M. Vaninsberghe, V. Bhardwaj and all members of the van Oudenaarden, Sonnen and Martinez Arias laboratories for discussions.

Author contributions S.C.v.d.B. and A.v.O. conceived and designed the project. S.C.v.d.B. and V.v.B. generated gastruloids, and S.C.v.d.B., M.B. and J.V. performed scRNA-seq experiments. Embedding of mouse gastruloids for tomo-seq was done by S.C.v.d.B. N.M. and P.B.-J. embedded mouse embryos for tomo-seq, with help from J.N. S.C.v.d.B. cryosectioned gastruloids and embryos, and performed tomo-seq experiments. J.V. developed the robotized tomo-seq protocol. A.A. performed the mapping and analysis, including comparisons with embryonic datasets, of the scRNA-seq and tomo-seq data. A.v.O. performed the linearized UMAP analysis. S.C.v.d.B., M.B., A.A., N.M. and A.M.A. interpreted the sequencing datasets. P.B.-J. performed the first Matrigel-embedding pilot experiments. V.v.B. performed time-lapse imaging experiments, in situ hybridization and HCR stainings, with help from S.C.v.d.B. and K.F.S. V.v.B. analysed the microscopy data, with support from K.F.S. V.v.B., S.C.v.d.B., A.v.O. and K.F.S. interpreted the imaging results. S.C.v.d.B., A.A., V.v.B. and A.v.O. wrote the manuscript with support from K.F.S. and A.M.A., and A.M.A. and A.v.O. guided the project.

Competing interests The authors declare no competing interests.

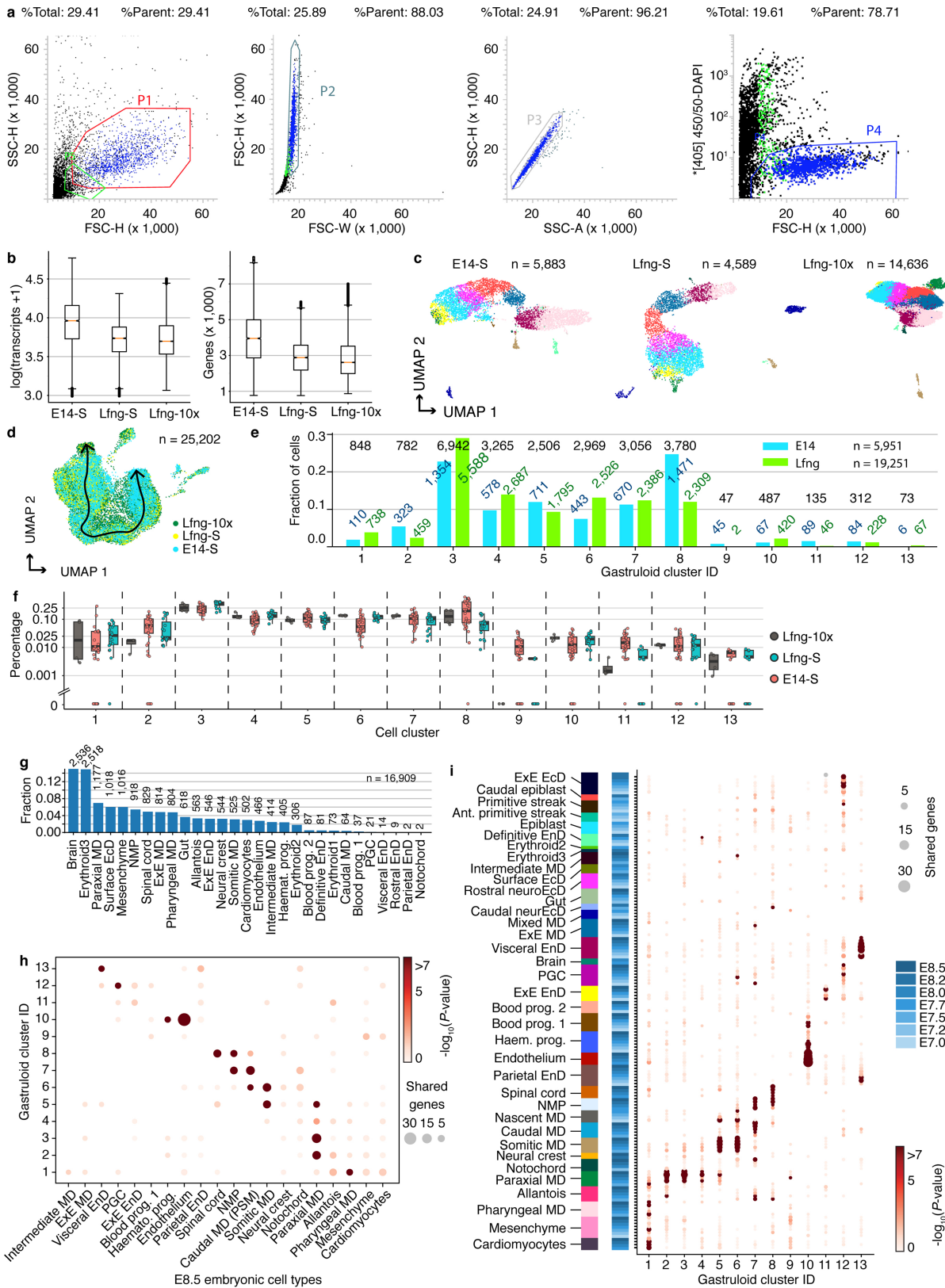
Additional information

Supplementary information is available for this paper at <https://doi.org/10.1038/s41586-020-2024-3>.

Correspondence and requests for materials should be addressed to S.C.v.d.B. or A.v.O.

Peer review information *Nature* thanks Jianping Fu and the other, anonymous, reviewer(s) for their contribution to the peer review of this work.

Reprints and permissions information is available at <http://www.nature.com/reprints>.



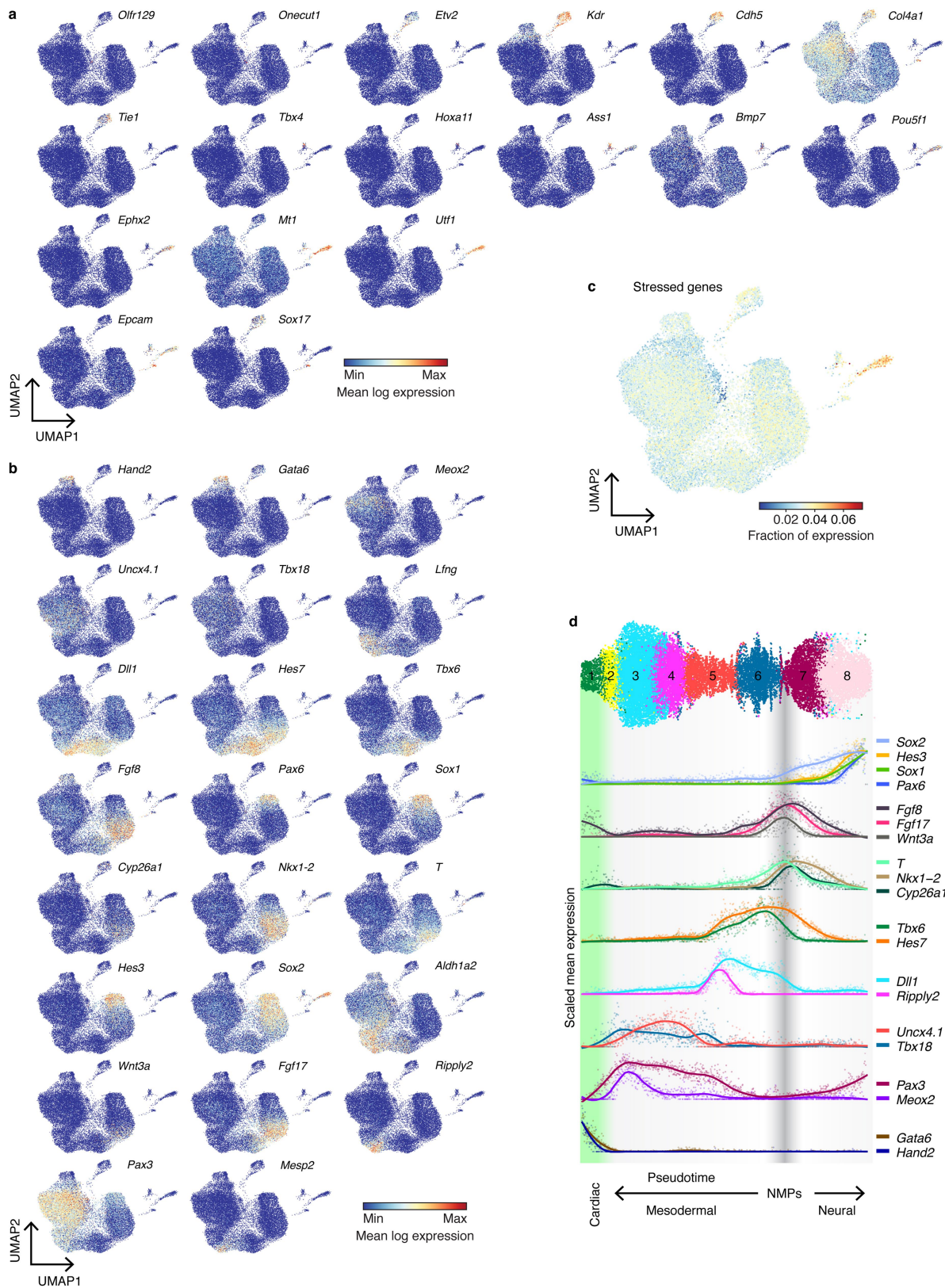
Extended Data Fig. 1 | See next page for caption.

Article

Extended Data Fig. 1 | scRNA-seq on 120-h mouse gastruloids and comparison to embryos.

a, FACS gating strategy before scRNA-seq. Live cells were selected on the basis of DAPI staining. Four sequential gates (P1–P4) were used; cells from gate P4 were used for scRNA-seq. SSC, side scatter; FSC, forward scatter; H, height; W, width; A, area. **b**, Box plot showing the median number of transcripts (left) and genes (right) detected per cell for SORT-seq experiments on E14-IB10 (E14-S, $n = 5,951$ cells from 26 biologically independent samples) and LfngT2AVenus gastruloids (Lfng-S, $n = 4,592$ cells from 74 biologically independent samples), and for 10x Genomics experiments on LfngT2AVenus gastruloids (Lfng-10x, $n = 14,659$ cells from 74 biologically independent samples). SORT-seq and 10x Genomics analyses were performed in parallel on the same 74 biologically independent LfngT2AVenus gastruloids; all cells extracted from these gastruloids were pooled and split into two tubes, of which one was used for SORT-seq and the other for 10x Genomics. The box extends from the lower to the upper quartile; whiskers are $1.5 \times$ the interquartile range; flier points are those past the end of the whiskers. **c**, UMAP plot for each experiment separately ($n = 5,883$, $4,589$ and $14,636$ cells for E14-S, Lfng-S and Lfng-10x, respectively; Methods). The E14-S cells ($n = 5,883$) were extracted from $n = 26$ biologically independent samples; the Lfng-S and Lfng-10x cells ($n = 4,589$ and $14,636$, respectively) were extracted from $n = 74$ biologically independent samples that were pooled and then split into one tube for SORT-seq and one tube for 10x Genomics. The colour of each cell is the same as the colour of that particular cell in Fig. 1a. **d**, UMAP plot obtained by analysing all the cells from the different experiments together ($n = 25,202$ cells from 100 biologically independent samples), in which cells are coloured according to their batch (Methods, Supplementary Table 1). The black line indicates the symmetry line in clusters 1–8 used to generate the linearized UMAP plot in Extended Data Fig. 2d (Methods). **e**, Fraction of E14-IB10 ($n = 26$ biologically independent samples) and LfngT2AVenus ($n = 74$ biologically independent samples) cells in each scRNA-seq cluster from Fig. 1a. Blue, green and black numbers, number of E14-IB10, LfngT2AVenus and total cells in each cluster, respectively (Supplementary Tables 1, 4). **f**, Fraction of cells for each cell type in each plate in SORT-seq experiments (Lfng-S, $n = 19$ plates containing cells from $n = 74$ biologically independent gastruloids; E14-S, $n = 30$ plates containing cells

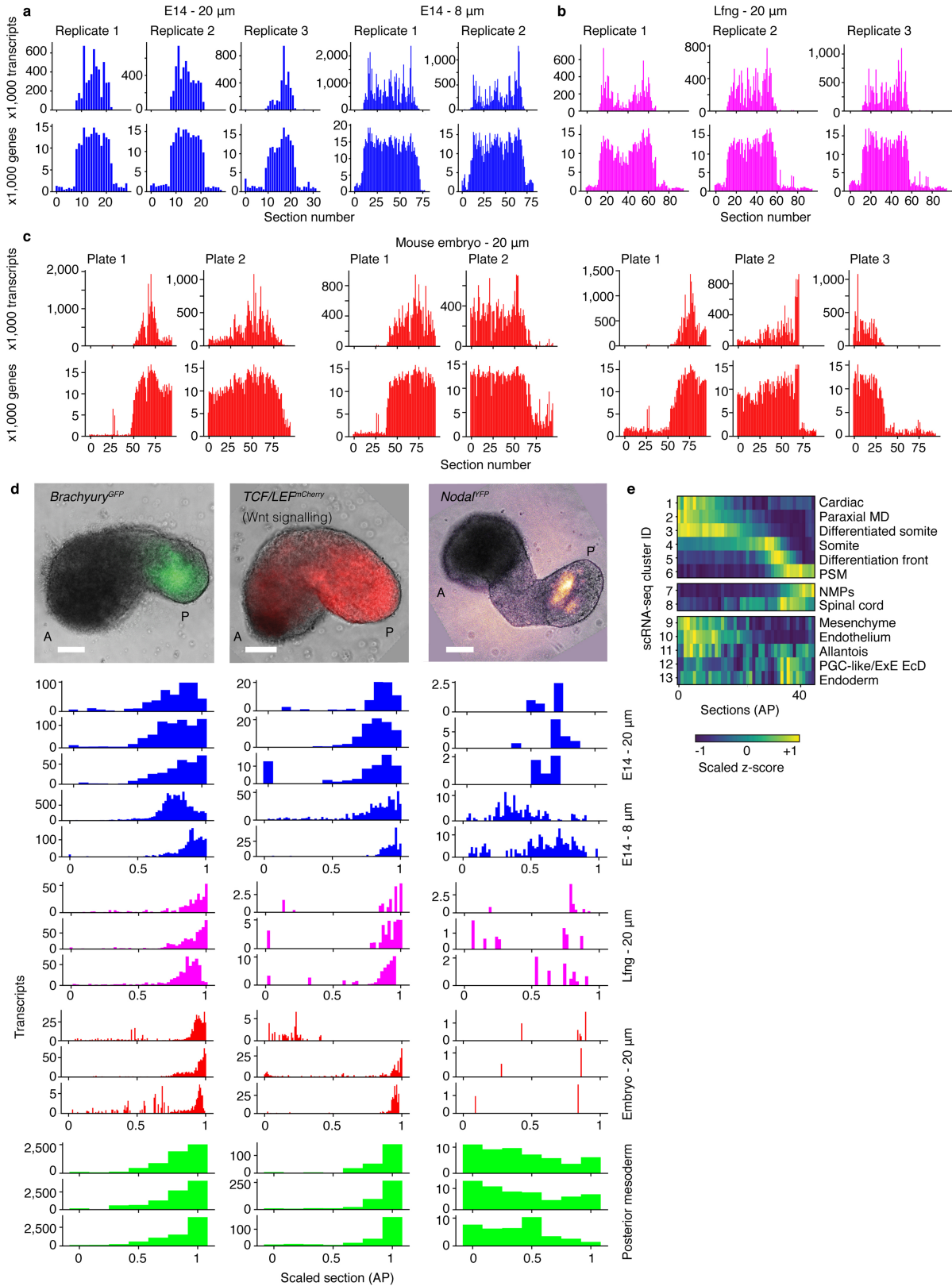
from $n = 26$ biologically independent gastruloids), and in each experimental batch in 10x Genomics experiments (Lfng-10x, $n = 2$ independent batches containing cells extracted from $n = 44$ and 30 biologically independent gastruloids, respectively, with 2 technical replicates each). In the box plots, centre line is median; box limits are the 1st and 3rd quartiles; and whiskers denote the range. **g**, Fraction of cells detected in the E8.5 mouse embryo scRNA-seq dataset⁴ with which we compared our gastruloid scRNA-seq data. Exact numbers in each cluster are indicated. **h**, Dot plot showing the number of overlapping genes between significantly upregulated genes ($n = 79, 87, 84, 22, 84, 66, 82, 78, 100, 97, 100, 96$ and 90 genes for clusters 1, 2, 3, 4, 5, 6, 7, 8, 9, 10, 11, 12 and 13 (respectively) in the gastruloid dataset, determined using the two-side t -test, followed by selection of genes with fold change above 1.01 and P value below 0.01; $n = 7, 20, 21, 35, 200, 39, 23, 200, 200, 95, 54, 21, 58, 57, 200, 81, 135, 28, 200$ and 200 genes for the embryonic-cell types reported in the x axis, determined in ref. ⁴ and selecting genes with P value below 0.01) for each gastruloid cluster ($n = 25,202$ cells extracted from 100 biologically independent samples) and each E8.5 mouse embryonic-cell type⁴. Dot colour indicates the probability of finding such a number of overlapping genes between the two sets by random chance (P value determined by binomial testing, one-sided, no adjustments for multiple corrections were made). Dot size represents the number of overlapping genes. **i**, Dot plot showing overlapping genes between significantly upregulated genes for each gastruloid scRNA-seq cluster ($n = 79, 87, 84, 22, 84, 66, 82, 78, 100, 97, 100, 96$ and 90 genes for clusters 1, 2, 3, 4, 5, 6, 7, 8, 9, 10, 11, 12 and 13, respectively (Supplementary Table 2); scRNA-seq dataset obtained for 25,202 cells that were extracted from $n = 100$ biologically independent gastruloids), and upregulated genes for each E7.0–E8.5 mouse embryonic-cell type⁴. Dot colour indicates the probability of finding such a number of overlapping genes between the two sets by random chance (P value determined by binomial testing, one-sided, no adjustments for multiple corrections were made), and dot size represents the number of overlapping genes. Blue, embryonic stage. 10x, 10x Genomics; Ant, anterior; EnD, endoderm; haemato, haemato-endothelial; prog, progenitors; S, SORT-seq³³.



Article

Extended Data Fig. 2 | Expression of relevant markers in the gastruloid scRNA-seq dataset. **a**, Mean log expression of relevant markers of outlier populations (clusters 9–13) plotted on the UMAP plot from Fig. 1a. *Olfir129* and *Onecut1*, head mesenchyme (cluster 9); *Etv2*, haemato-endothelial progenitors (bottom part of cluster 10); *Kdr*, haemato-endothelial progenitors and endothelium (cluster 10); *Cdh5* and *Tie1*, endothelium (top part of cluster 10); *Tbx4*, *Hoxa11*, *Ass1* and *Bmp7*, allantois (cluster 11); *Ephx2*, *Mt1*, *Utf1* and *Pou5f1*, primordial-germ-cell-like or extra-embryonic ectoderm (cluster 12); *Col4a1*, *Epcam* and *Sox17*, endoderm (cluster 13). **b**, Mean log normalized expression of relevant markers of clusters 1–8 plotted on the UMAP plot from Fig. 1a. *Hand2* and *Gata6*, heart (cluster 1); *Meox2* and *Pax3*, differentiated somite (cluster 3); *Aldh1a2* and *Uncx4.1*, somite (cluster 4); *Lfng*, *Mesp2*, *Ripply2* and *Dll1*, differentiation front (cluster 5); *Hes7* and *Tbx6*, presomitic mesoderm

(cluster 6); *Wnt3a*, *Fgf17*, *Fgf8*, *Cyp26a1*, *Nkx1-2* and *T*, tail bud containing neuromesodermal progenitors (cluster 7); *Pax6*, *Sox1*, *Hes3* and *Sox2*, differentiated neural cells (spinal cord; cluster 8). Expression was first count-normalized to 10,000 for each cell (Methods), and then log-transformed. Additional markers of all clusters are provided in Supplementary Table 2. **c**, Percentage of total unique transcripts per cell corresponding to stress genes⁴² plotted on the UMAP plot from Fig. 1a. **d**, Linearized UMAP plot of clusters 1–8 (top, $n = 24,148$ cells, isolated from 100 biologically independent gastruloids during $n = 6$ independent experiments) and expression profiles of genes related to neural and mesodermal differentiation^{8,9} (bottom). Green and grey shades indicate location of cardiac cells and neuromesodermal progenitors, respectively. The position of each cell along the x-axis relates to its differentiated state towards a neural or mesodermal fate.



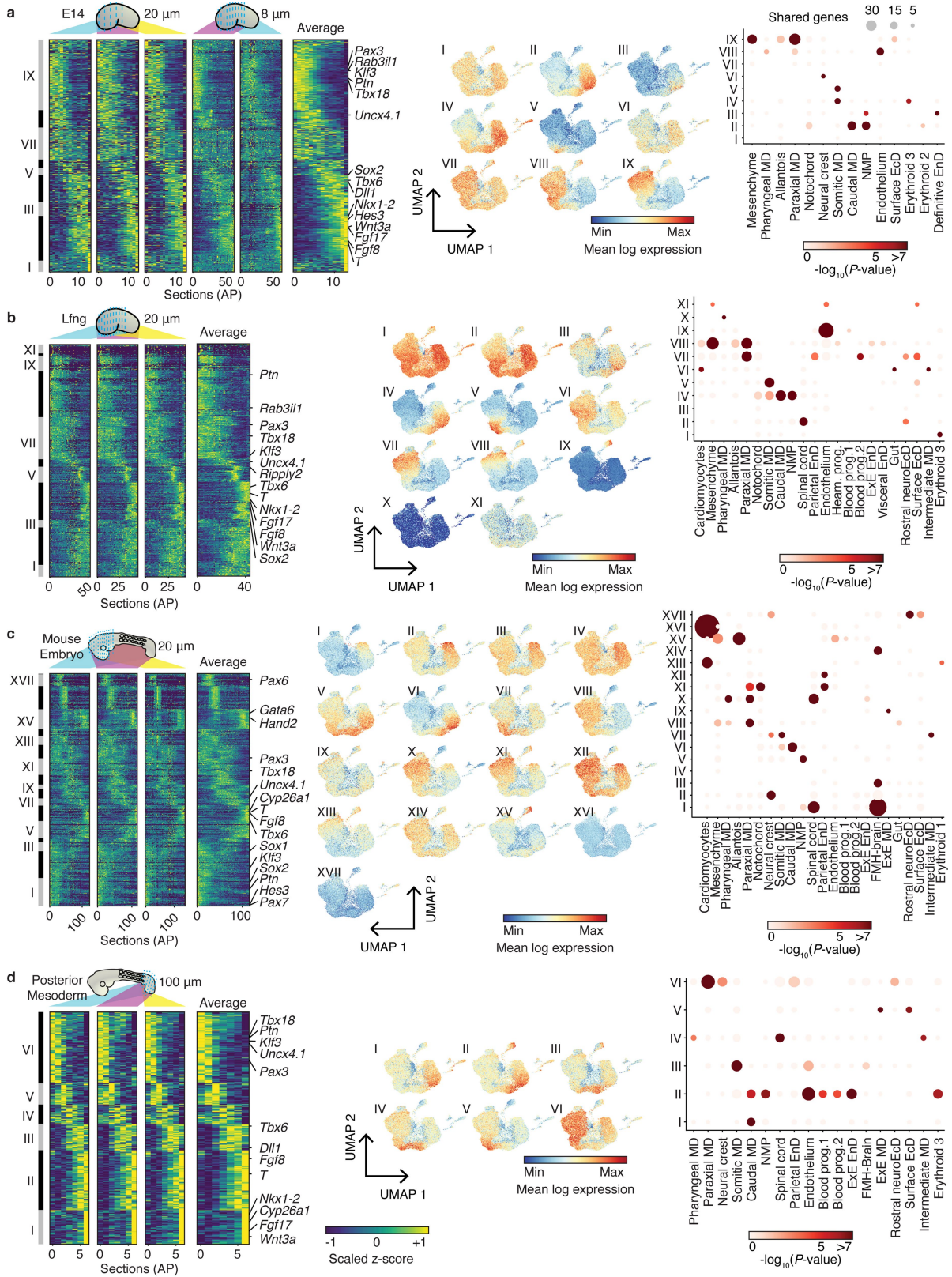
Extended Data Fig. 3 | See next page for caption.

Article

Extended Data Fig. 3 | The number of genes and reads in gastruloid and embryo tomo-seq datasets, and comparison to microscopy data.

a–c, Number of unique transcripts and genes detected in 3 E14-IB10 120-h mouse gastruloids that were sectioned using 20- μm sections and 2 E14-IB10 120-h mouse gastruloids that were sectioned using 8- μm sections (**a**); in 3 LfngT2AVenus 120-h mouse gastruloids that were sectioned using 20- μm sections (**b**); and in 3 E8.5 mouse embryos that were sectioned using 20- μm sections (**c**). Owing to their lengths, embryo sections were collected in 2 or 3 sequential 96-well plates. **d**, Validation of tomo-seq data with microscopy. Top panels, *Brachyury-GFP*, WNT signalling activity (as reported using a TCF/LEF-*mCherry* mouse ES cell line) and *Nodal-YFP* expression in 120-h mouse

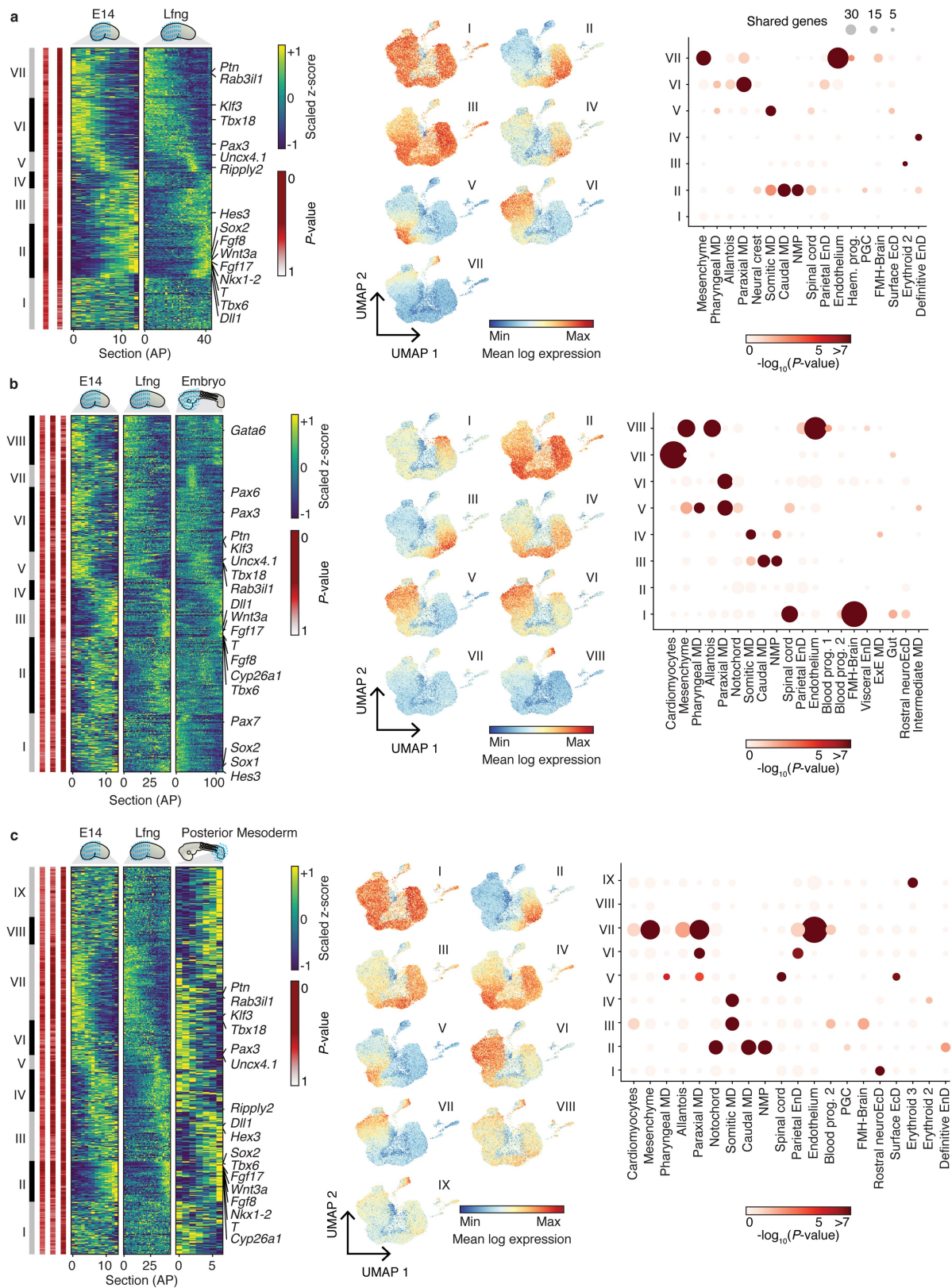
gastruloids as measured by microscopy (Methods). With each reporter line, we obtained similar results in $n = 5$ independent experiments. Bar plots show the normalized expression levels of *Brachyury*, *Wnt3a* and *Nodal* in 120-h E14-IB10 gastruloids, 120-h LfngT2AVenus gastruloids and E8.5 mouse embryos as determined by tomo-seq (Methods), and in the posterior mesoderm of E9.5 mouse embryos as determined by microarray¹². **e**, Scaled average z-score of significantly upregulated genes (P value < 0.01 and \log_2 -transformed fold change > 1.01) detected in each single-cell cluster from Fig. 1a (Supplementary Table 2) as measured in the averaged LfngT2AVenus tomo-seq gastruloid. Scale bar, 100 μm .



Extended Data Fig. 4 | See next page for caption.

Extended Data Fig. 4 | Individual replicates of gastruloids, E8.5 embryo tomo-seq and E9.5 posterior mesoderm datasets, and comparison to gastruloid and E8.5 embryonic scRNA-seq datasets. **a**, Heat maps showing the anterior–posterior expression patterns of 1,199 genes as detected by tomo-seq¹¹ in individual replicates of 120-h E14-IB10 gastruloids ($n = 3$ gastruloids, 20- μm sections and $n = 2$ gastruloids, 8- μm sections) that were cultured in standard^{1,20} (non-Matrigel-based) conditions; average heat map of the five replicates; average expression of genes found in each tomo-seq domain in the E14-IB10 tomo-seq dataset, projected in the UMAP plot from Fig. 1a; dot plot showing overlapping genes between genes detected in each tomo-seq domain in the E14-IB10 tomo-seq dataset, and upregulated genes for each E8.5 mouse embryonic-cell type⁴. Dot colour represents the probability of finding such a number of overlapping genes between the two sets by random chance (Methods), and dot size represents the number of overlapping genes. Only genes that were reproducible between replicates are shown (Methods). Genes are clustered on the basis of their anterior–posterior expression pattern

(Methods); bars marked with Roman numerals represent tomo-seq clusters. Clusters I, II, III, IV, V, VI, VII, VIII and IX contain $n = 58, 231, 72, 138, 38, 43, 165, 90$ and 364 genes, respectively. **b**, Similar to **a**, but for 1,456 genes in 120-h LfngT2AVenus¹⁵ ($n = 3$ gastruloids, 20- μm sections) gastruloids that were cultured in standard^{1,20} (non-Matrigel-based) conditions. Clusters I, II, III, IV, V, VI, VII, VIII, IX, X and XI contain $n = 74, 235, 47, 235, 99, 47, 264, 287, 99, 14$ and 55 genes, respectively. **c**, Similar to **a**, but for 1,553 genes in E8.5 embryos ($n = 3$ embryos, 20- μm sections). Clusters I, II, III, IV, V, VI, VII, VIII, IX, X, XI, XII, XIII, XIV, XV, XVI, XVII, XVIII and XIX contain $n = 186, 179, 63, 25, 114, 103, 48, 65, 28, 65, 111, 89, 61, 44, 134, 155, 79, 2$ and 2 genes, respectively. **d**, Similar to **a**, but for 1,989 genes in an E9.5 mouse embryo posterior-mesoderm dataset (tail bud to newly formed somite) ($n = 3$ embryos; previously published microarray data; approximately 100- μm sections¹²). Clusters I, II, III, IV, V and VI contain $n = 294, 512, 226, 165, 181$ and 611 genes, respectively. All genes are shown in Supplementary Table 6. AP, anterior–posterior; FMH, fore-, mid- and hind-



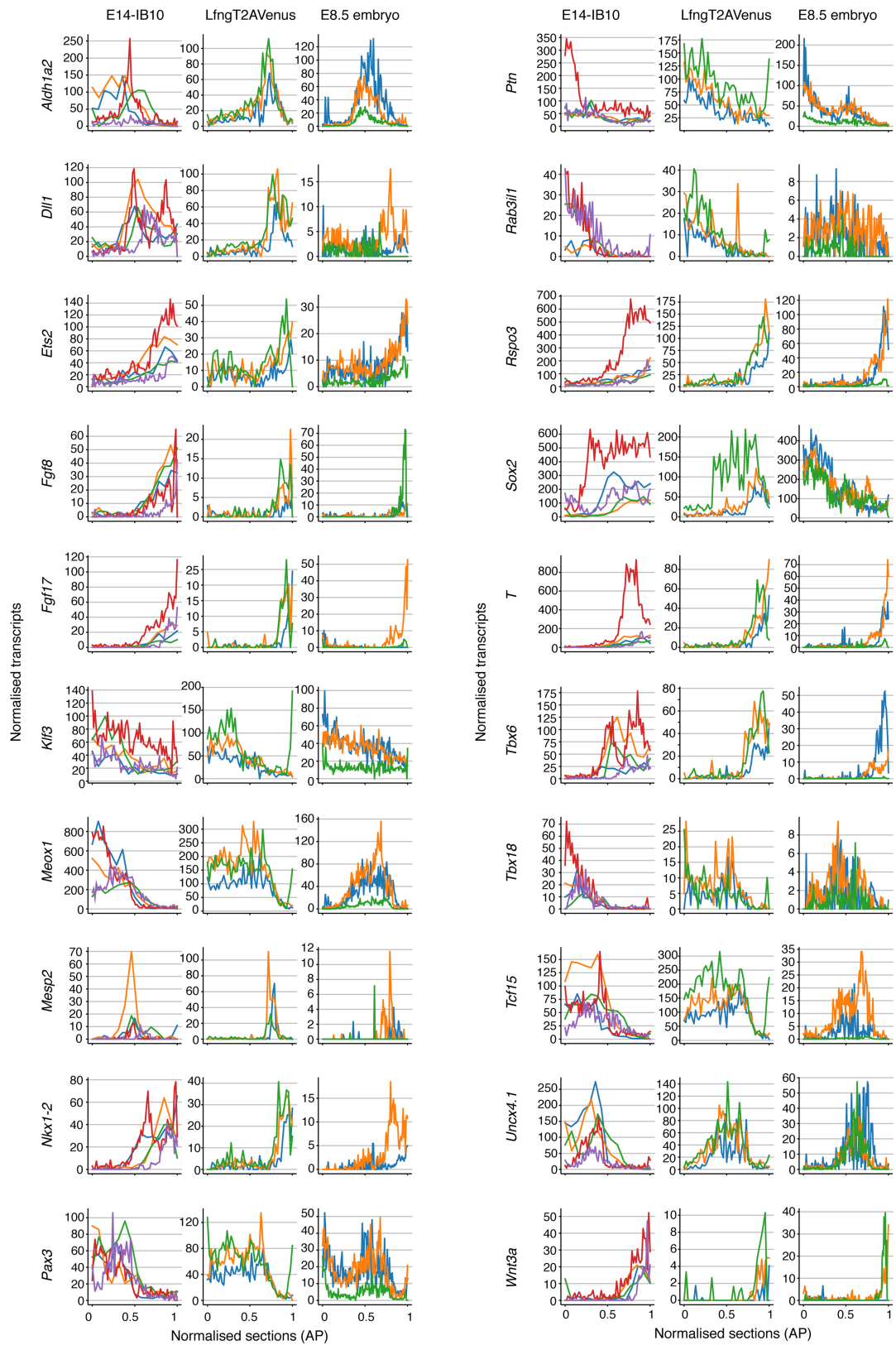
Extended Data Fig. 5 | See next page for caption.

Article

Extended Data Fig. 5 | Comparisons between mouse gastruloid and mouse embryo datasets, including genes that are reproducible in at least one system.

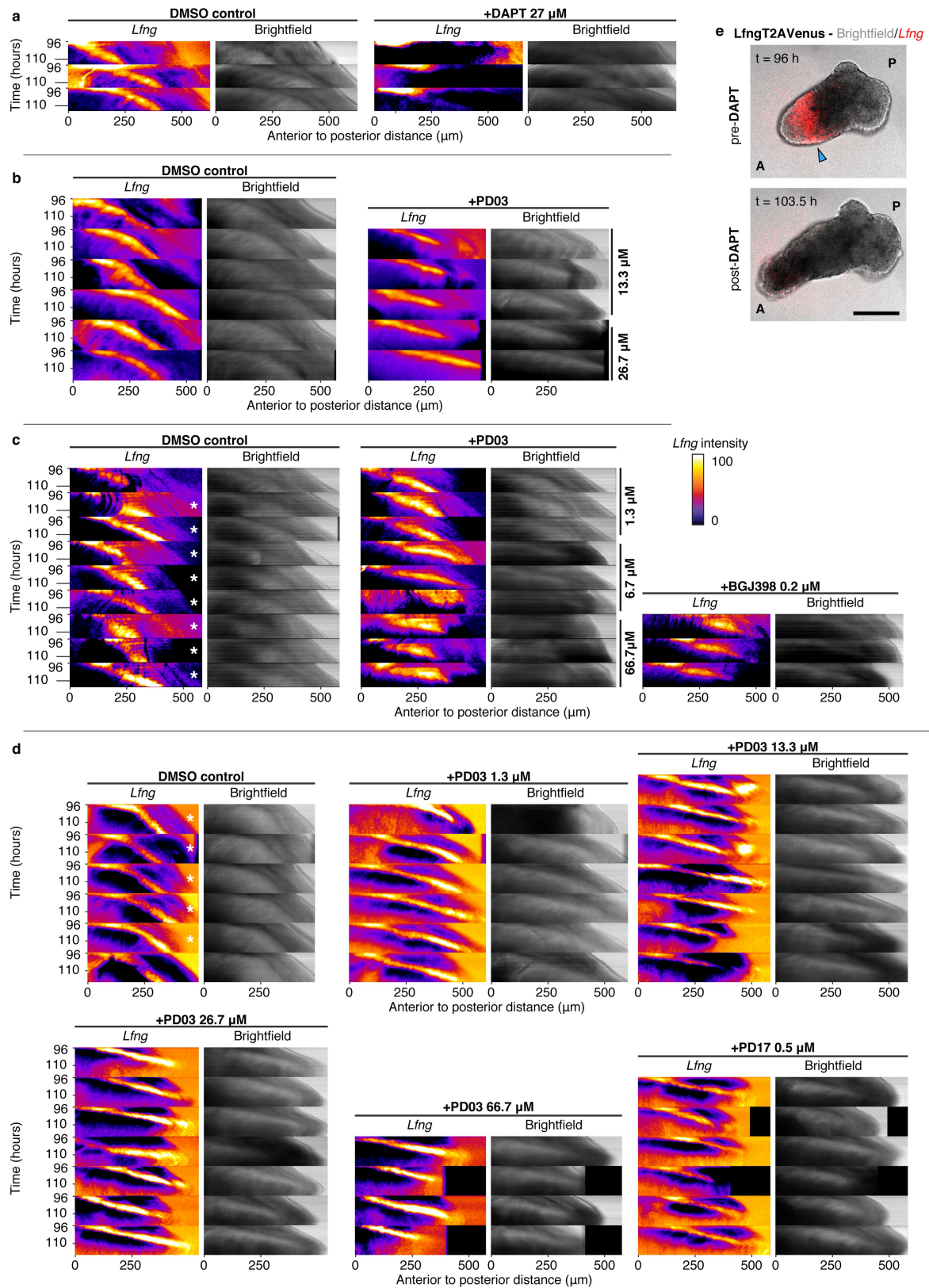
a. Heat map showing the average anterior–posterior expression pattern of 2,065 genes as detected by tomo-seq¹¹ in 120-h mouse gastruloids that were generated from E14-IB10 and LfngT2AVenus¹⁵ mouse ES cells and that were cultured in standard^{1,20} (non-Matrigel-based) conditions; average expression of genes found in each tomo-seq domain in the E14-IB10–LfngT2AVenus comparison heat map, projected in the UMAP plot from Fig. 1a; dot plot showing overlapping genes between genes detected in each tomo-seq domain in **a**, and upregulated genes for E8.5 mouse embryonic-cell types⁴. Dot colour represents the probability of finding such a number of overlapping genes by random chance (Methods), and dot size represents the number of overlapping genes. In contrast to the heat maps in Fig. 1, this heat map contains genes that were reproducible in either E14-IB10 ($n = 3$ biologically independent gastruloids, 20- μm sections and $n = 2$ biologically independent gastruloids, 8- μm sections) or LfngT2AVenus ($n = 3$ biologically independent gastruloids, 20- μm sections) gastruloids (Extended Data Fig. 4, Methods, Supplementary Tables 5, 6). This means that genes that are reproducible in E14-IB10 replicates but not in LfngT2AVenus replicates—and vice versa—are included. Genes are

clustered on the basis of their anterior–posterior expression pattern (Methods); bars marked by Roman numerals represent tomo-seq clusters, which are also indicated with the grey–black bar plot. The red-to-white bar plots indicate the P value of reproducibility of each gene in each heat map. The order of these bar plots corresponds to the order of the heat maps. Clusters I, II, III, IV, V, VI and VII contain $n = 377, 398, 259, 124, 145, 395$ and 367 genes, respectively. **b.** Similar to **a**, but for 2,894 genes that were reproducible in E14-IB10 ($n = 3$ gastruloids, 20- μm sections and $n = 2$ gastruloids, 8- μm sections) or LfngT2AVenus ($n = 3$ gastruloids, 20- μm sections) or E8.5 mouse embryos ($n = 3$ embryos, 20- μm sections). Clusters I, II, III, IV, V, VI, VII and VIII contain $n = 477, 618, 302, 161, 230, 527, 179$ and 400 genes, respectively. **c.** Similar to **a**, but for 3,086 genes that were reproducible in E14-IB10 ($n = 3$ gastruloids, 20- μm sections and $n = 2$ gastruloids, 8- μm sections) or LfngT2AVenus ($n = 3$ gastruloids, 20- μm sections) or the E9.5 mouse embryo posterior-mesoderm dataset (tail bud to newly formed somite) ($n = 3$ embryos; previously published microarray data; approximately 100- μm sections¹²). Clusters I, II, III, IV, V, VI, VII, VIII and IX contain 419, 325, 392, 337, 114, 279, 602, 220 and 398 genes, respectively. Gene lists are provided in Supplementary Table 8.



Extended Data Fig. 6 | Gene-expression profiles in gastruloid and embryo tomo-seq datasets. Line plots for the normalized anterior–posterior expression of genes emphasized in Fig. 1b, d, e for the E14-IB10 and

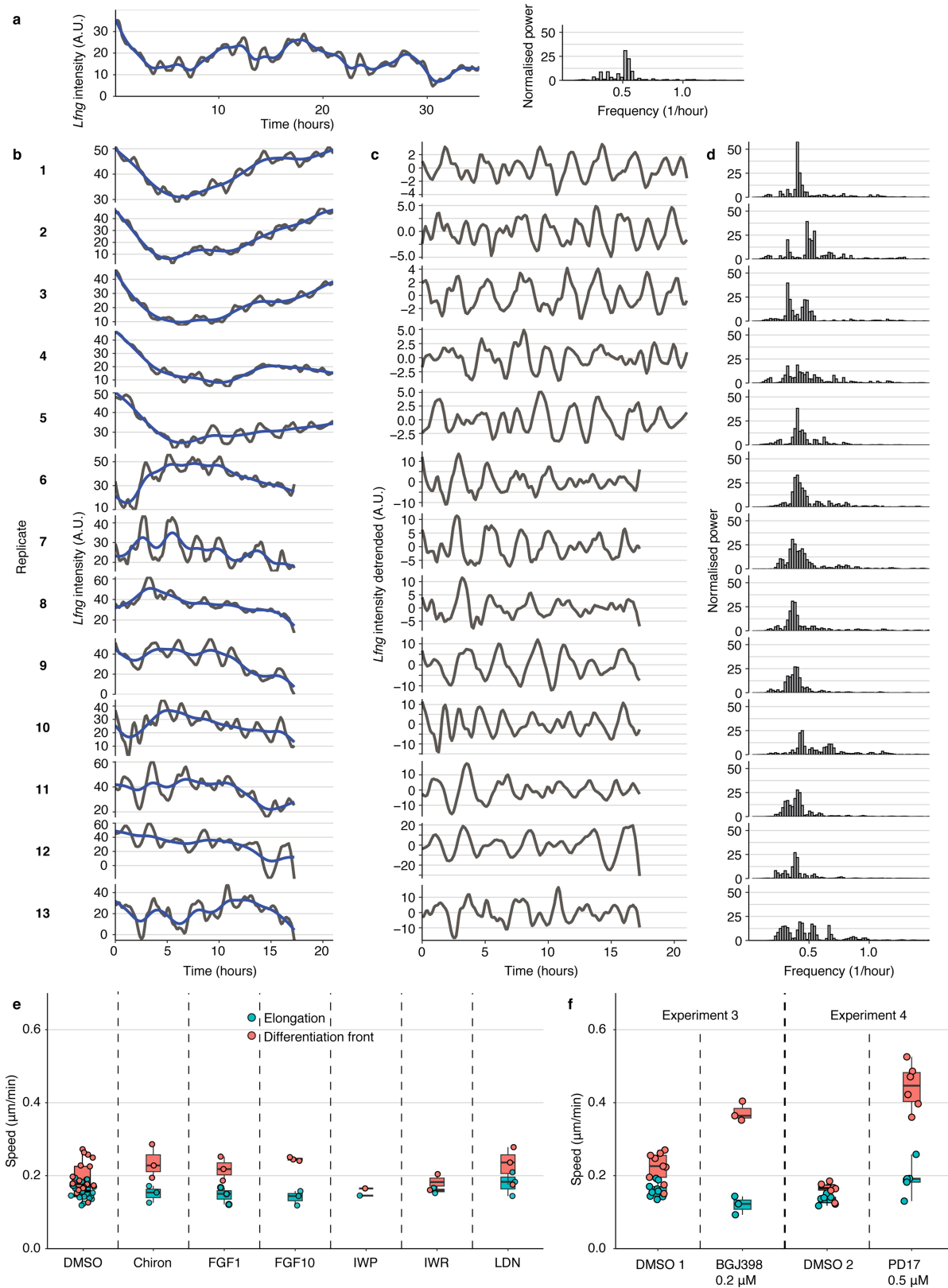
LfngT2AVenus gastruloids, and for the E8.5 mouse embryo, as measured by tomo-seq¹¹. Each colour denotes a different replicate.



Extended Data Fig. 7 | See next page for caption.

Extended Data Fig. 7 | Kymographs of time-lapse experiments performed on LfngT2AVenus gastruloids that were embedded in 100% Matrigel at 96 h. **a–d**, Kymographs (space–time plots) of bright field channel and LfngT2AVenus signal along the anterior–posterior axis of all replicates from all time-lapse experiments (experiments 1–4) that are presented in Fig. 2e, Extended Data Fig. 8e, f. These gastruloids were embedded in 100% Matrigel (Methods) to stabilize them during imaging, and subsequently imaged for at least 17 h (Supplementary Videos 1, 2, 4, 5). Inhibitors were added at the start of the time lapse (Methods) and are indicated above the kymographs, together with their

concentration. Asterisks refer to gastruloids used to generate Fig. 2e, Extended Data Fig. 8b–d. Similar results were obtained in $n = 5$ and 4 independent experiments for **a** and **b–d**, respectively. **e**, Imaging of a LfngT2AVenus gastruloid that was embedded in 100% Matrigel at 96 h, and to which the Notch inhibitor DAPT was added at 96.5 h (Supplementary Video 2); the *Lfng* signal disappears about 6 h after addition of DAPT. Corresponding kymographs in **a**. Similar results were obtained in $n = 5$ independent experiments. Scale bar, 200 μm .

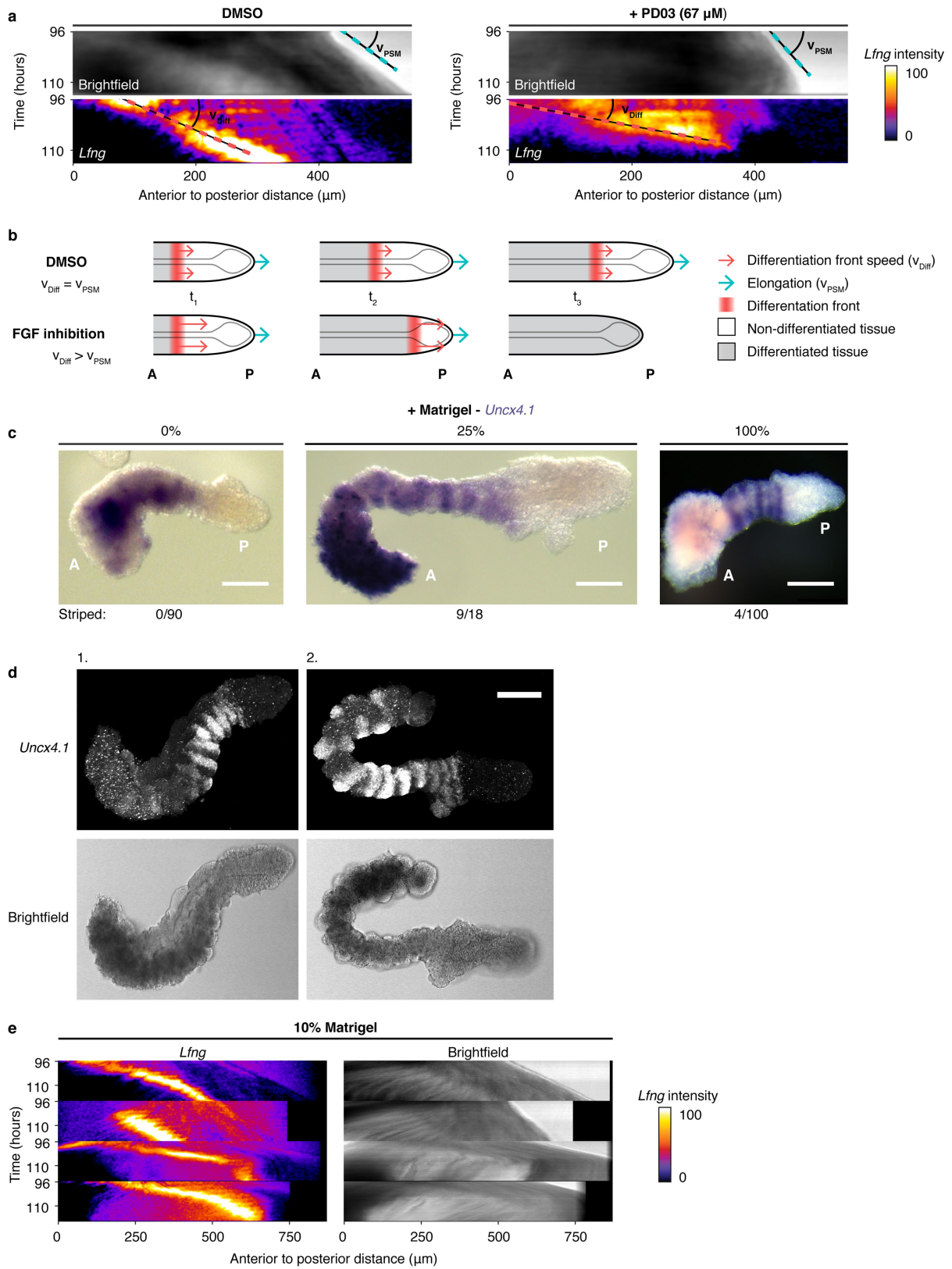


Extended Data Fig. 8 | See next page for caption.

Extended Data Fig. 8 | Detrending procedure and Lomb–Scargle analysis of replicates, as well as measurements of elongation and differentiation front speed in small panel screening, and upon BGJ389 and PD17 treatment.

Replicates subjected to detrending and Lomb–Scargle analysis are from Fig. 2. **a**, Black line, measured intensity of the *Lfng* signal along the white dashed line in Fig. 2c; blue line, trend (Methods) of this signal and periodogram of the *Lfng* oscillations in Fig. 2d, as determined by Lomb–Scargle decomposition. **b**, As in **a**, but then for the 13 DMSO-control *LfngT2AVenus* gastruloid replicates shown in Extended Data Fig. 7c, d. **c**, Cyclical component of the scaled intensity of the *LfngT2AVenus* oscillations relative to the trend line shown in **b**. A.U., arbitrary units. **d**, Periodogram of the *Lfng* oscillations in **c**, as determined by Lomb–

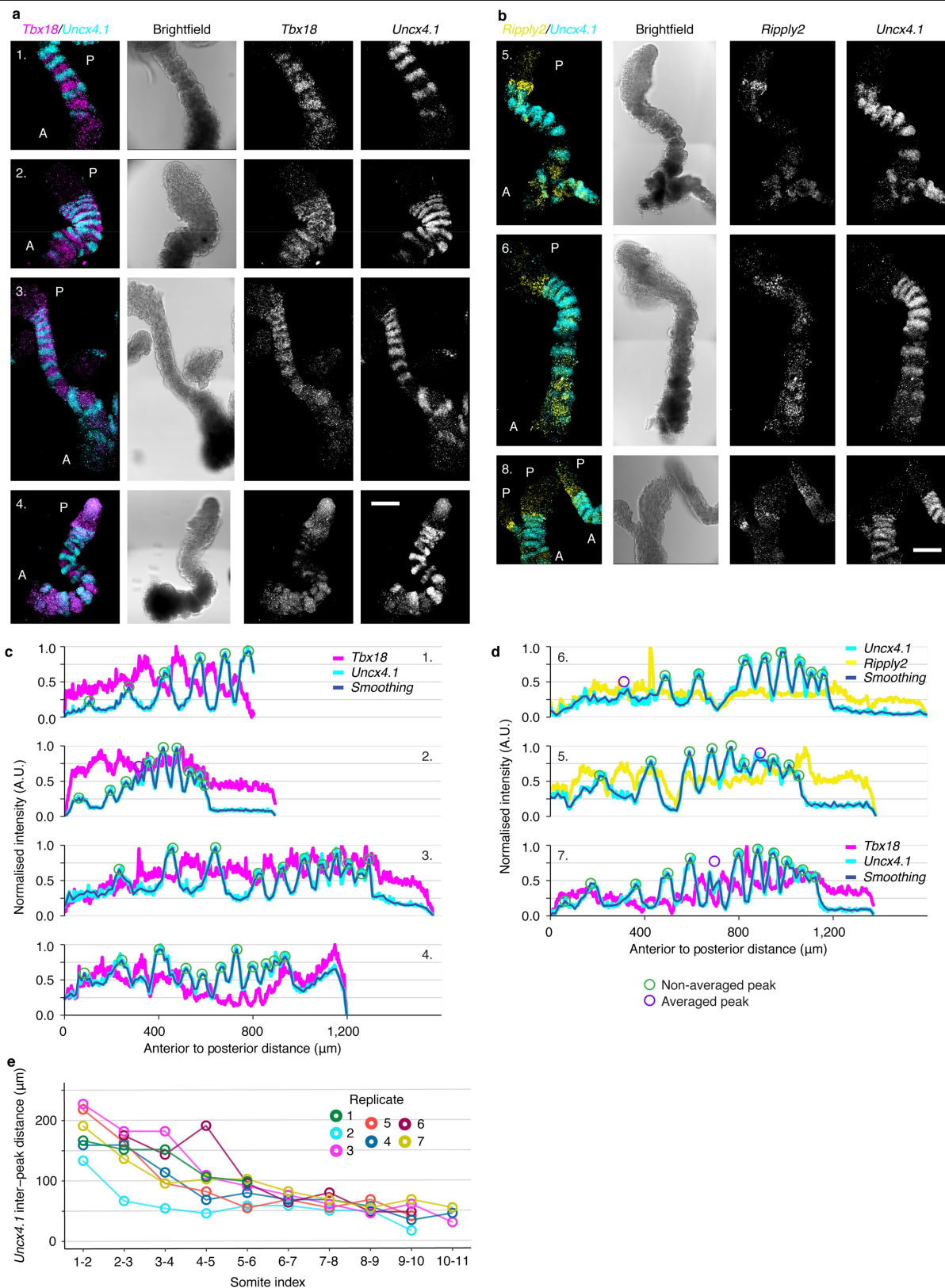
Scargle decomposition (Methods). Gastruloids used for this experiment were embedded in 100% Matrigel at 96 h, and subsequently imaged for at least 17 h. **e, f**, Speed of posterior gastruloid elongation (V_{PSM}) and speed of posteriorly moving differentiation front (V_{DIFF}) (see explanation in Extended Data Fig. 9a) in *LfngT2AVenus* gastruloids treated with DMSO (control) or with various inhibitors (Supplementary Videos 3, 5). Points refer to replicates; $n = 14, 3, 3, 3, 1, 2$ and 3 (from left to right) and $9, 3, 6$ and 6 (from left to right) replicates for **e** and **f**, respectively. Kymographs of replicates are shown in Extended Data Fig. 7. In the box plots, centre line is median; box limits are the 1st and 3rd quartiles; and whiskers denote the range.



Extended Data Fig. 9 | See next page for caption.

Extended Data Fig. 9 | Explanation for how elongation and differentiation-front speed were measured, and HCR stainings and kymographs of gastruloids embedded in 10% Matrigel. **a**, Kymographs (space–time plots) of bright field channel and LfngT2AVenus signal along the anterior–posterior axis of a DMSO-treated (control) and a PD03 (MEKinhibitor)-treated LfngT2AVenus gastruloid. Gastruloids were embedded in 100% Matrigel at 96 h; DMSO or PD03 (66.7 μ M) was added at 96.5 h. Kymographs were used to measure the elongation speed of the gastruloid (angle of blue dashed line; V_{PSM}) (Methods) and the speed of the differentiation front (angle of red dashed line; V_{DIFF}). Similar results were obtained in $n = 4$ independent experiments. **b**, Illustration explaining the effect of FGF inhibition, which increases the speed of the differentiation front (red arrows, V_{DIFF}) without altering the elongation rate (blue arrows, V_{PSM}) of gastruloids. Three time points (t_1 , t_2 and t_3) are depicted. White tissue, nondifferentiated tissue (presomitic mesoderm); grey tissue,

differentiated tissue. **c**, In situ hybridization staining for *Uncx4.1* on 120-h LfngT2AVenus gastruloids that were not embedded in Matrigel (0%) (standard, previously published protocol^{1,20}) or that were embedded in 25% or 100% Matrigel at 96 h. Numbers below the panels indicate the number of gastruloids in which stripy *Uncx4.1* expression patterns were observed. Similar results were obtained in $n = 3$ independent experiments. **d**, LfngT2AVenus gastruloids that were embedded in 10% Matrigel (Methods) at 96 h and stained for *Uncx4.1* using HCR²¹ at 120 h. A magnified view of the left gastruloid is shown in Fig. 3a. Similar results were obtained in $n = 5$ independent experiments. **e**, Kymographs of LfngT2AVenus signal and bright field channel along the anterior–posterior axis of gastruloids that were embedded in 10% Matrigel at 96 h, and subsequently imaged for 20 h (Supplementary Video 6). Top kymograph belongs to the gastruloid that is shown in Fig. 3b. Similar results were obtained in $n = 2$ independent experiments. Scale bars, 200 μ m.



Extended Data Fig. 10 | *Uncx4.1* *Tbx18* *Ripply2* stainings and somite-size measurements. **a**, HCR²¹ double staining for *Uncx4.1* (cyan) and *Tbx18* (magenta) on 120-h LfngT2Avenus gastruloids embedded in 10% Matrigel at 96 h. For replicate 4, 1.3 μM of PD03 was added at 96.5 h. Similar results were obtained in $n = 4$ independent experiments. **b**, Similar to **a**, but for *Uncx4.1* (cyan) and *Ripply2* (yellow). Similar results were obtained in $n = 2$ independent experiments. **c**, Intensity of *Uncx4.1* and *Tbx18* signal along the anterior–

posterior axis of the gastruloids in **a**. Peaks (circles) are called on the smoothed *Uncx4.1* profile (dark blue) (Methods). **d**, Similar to **c**, but for the *Uncx4.1*- and *Ripply2*-stained gastruloids from **b**. **e**, Distance between *Uncx4.1* peaks in the 120-h LfngT2Avenus gastruloids ($n = 7$) from replicates 1–6 in **a–d** and in replicate 7 (which is shown in Fig. 3c). Replicate 8 was excluded from quantification and both replicate 4 and replicate 7 were incubated in 1.3 μM PD03 from 96–120 h. Scale bars, 200 μm .

Reporting Summary

Nature Research wishes to improve the reproducibility of the work that we publish. This form provides structure for consistency and transparency in reporting. For further information on Nature Research policies, see [Authors & Referees](#) and the [Editorial Policy Checklist](#).

Statistics

For all statistical analyses, confirm that the following items are present in the figure legend, table legend, main text, or Methods section.

- | n/a | Confirmed |
|-------------------------------------|--|
| <input type="checkbox"/> | <input checked="" type="checkbox"/> The exact sample size (n) for each experimental group/condition, given as a discrete number and unit of measurement |
| <input type="checkbox"/> | <input checked="" type="checkbox"/> A statement on whether measurements were taken from distinct samples or whether the same sample was measured repeatedly |
| <input type="checkbox"/> | <input checked="" type="checkbox"/> The statistical test(s) used AND whether they are one- or two-sided <i>Only common tests should be described solely by name; describe more complex techniques in the Methods section.</i> |
| <input checked="" type="checkbox"/> | <input type="checkbox"/> A description of all covariates tested |
| <input type="checkbox"/> | <input checked="" type="checkbox"/> A description of any assumptions or corrections, such as tests of normality and adjustment for multiple comparisons |
| <input type="checkbox"/> | <input checked="" type="checkbox"/> A full description of the statistical parameters including central tendency (e.g. means) or other basic estimates (e.g. regression coefficient) AND variation (e.g. standard deviation) or associated estimates of uncertainty (e.g. confidence intervals) |
| <input type="checkbox"/> | <input checked="" type="checkbox"/> For null hypothesis testing, the test statistic (e.g. F , t , r) with confidence intervals, effect sizes, degrees of freedom and P value noted <i>Give P values as exact values whenever suitable.</i> |
| <input checked="" type="checkbox"/> | <input type="checkbox"/> For Bayesian analysis, information on the choice of priors and Markov chain Monte Carlo settings |
| <input checked="" type="checkbox"/> | <input type="checkbox"/> For hierarchical and complex designs, identification of the appropriate level for tests and full reporting of outcomes |
| <input type="checkbox"/> | <input checked="" type="checkbox"/> Estimates of effect sizes (e.g. Cohen's d , Pearson's r), indicating how they were calculated |

Our web collection on [statistics for biologists](#) contains articles on many of the points above.

Software and code

Policy information about [availability of computer code](#)

| | |
|-----------------|---|
| Data collection | For FACS, BD FACS software (version 1.2.0.124) was used. |
| Data analysis | scRNA-seq analysis was performed using custom-made code and the Scanpy package (v1.4.3) in Python 3.6. Reads were trimmed using TrimGalore (v0.4.3) and mapped using STAR (v2.5.3a). Batch-effects were removed using the combat function from Scanpy (v1.4.3), a Python implementation of the R-package Bioconductor. All code is available at https://github.com/anna-alemany/mouseGastruloids_scrNAseq_tomoseq . Tomo-seq analysis was performed with custom-made code in Python 3.6. All code is available at https://github.com/anna-alemany/mouseGastruloids_scrNAseq_tomoseq . Fiji (v2.0.0) and the plugins KymoResliceWide (v0.5) and Correlescence (v0.0.3) were used for microscopy data analysis. Measurements made during microscopy were analyzed in R (v3.6.1). Code is available at https://github.com/vincentvbatenburg/MouseGastruloids . |

For manuscripts utilizing custom algorithms or software that are central to the research but not yet described in published literature, software must be made available to editors/reviewers. We strongly encourage code deposition in a community repository (e.g. GitHub). See the Nature Research [guidelines for submitting code & software](#) for further information.

Data

Policy information about [availability of data](#)

All manuscripts must include a [data availability statement](#). This statement should provide the following information, where applicable:

- Accession codes, unique identifiers, or web links for publicly available datasets
- A list of figures that have associated raw data
- A description of any restrictions on data availability

All RNA-seq datasets produced in this study are deposited in the Gene Expression Omnibus (GEO) under accession code GSE123187. All scRNA-seq and tomo-seq data can be explored at <https://avolab.hubrecht.eu/MouseGastruloids2020>. The source data associated with Figs. 1 and 2 and Extended data Figs. 1-6, 8 and 10 are provided in the online version of the manuscript.

Field-specific reporting

Please select the one below that is the best fit for your research. If you are not sure, read the appropriate sections before making your selection.

- Life sciences Behavioural & social sciences Ecological, evolutionary & environmental sciences

For a reference copy of the document with all sections, see [nature.com/documents/nr-reporting-summary-flat.pdf](https://www.nature.com/documents/nr-reporting-summary-flat.pdf)

Life sciences study design

All studies must disclose on these points even when the disclosure is negative.

| | |
|-----------------|--|
| Sample size | The sample size was not predetermined for any of the experiments performed for this study. For the scRNA-seq experiments, we analyzed 25,202 cells isolated from 26 E14-IB10 and 74 LfngT2AVenus gastruloids that were generated during 6 independent experiments. These sample sizes allowed us to have an estimation of the variability in the cell type composition across gastruloids and across experiments. For tomo-seq experiments, we processed 5 gastruloids generated from E14-IB10 cells and 3 gastruloids generated from LfngT2AVenus cells, and 3 E8.5 mouse embryos. This sample size was sufficient as the gene expression patterns measured were highly reproducible between all replicates. For all live-imaging experiments, in situ hybridization stainings and HCR stainings performed in the study, the sample sizes are indicated in the figure legends. |
| Data exclusions | The following data-exclusions were pre-established: aggregates that did not elongate and that did not form gastruloids were excluded from the study. Curved gastruloids were excluded from tomo-seq experiments. Ribosomal and mitochondrial genes were removed from scRNA-seq and tomo-seq downstream analysis, together with Kcnq1ot1, Lars2 and Malat1, because these genes seem to be linked to mapping errors and have been shown to be erroneous in earlier studies from our lab. The following data-exclusions were not pre-established and were decided upon during data-analysis: for tomo-seq, 20 µm sectioned slides with less than 3,200 genes and 8 µm sectioned slices with less than 6,000 genes were filtered out as these sections are most likely empty and do not contain gastruloid material. For scRNA-seq analysis, cells with less than 3,000 total transcripts and genes with less than 3 normalized transcripts in a single cell are filtered out. |
| Replication | All results obtained in this study were reliably reproduced. During the study, we noticed that oscillations and somites were more reliably reproduced in gastruloids generated from cells with a low passage number. We have indicated this in the methods section. For all experiments, the frequencies of all reported observations are indicated in the figure legends. |
| Randomization | All gastruloids were randomly allocated the different experimental groups. |
| Blinding | Blinding was not relevant for the scRNA-seq or tomo-seq parts of this study, as no comparisons between different conditions were made in these experiments. For the experiments in which the effect of various concentrations of various inhibitors was tested, blinding was not relevant as the effect of these inhibitors on the dynamics of the differentiation front were measured in an automated, unbiased manner. |

Reporting for specific materials, systems and methods

We require information from authors about some types of materials, experimental systems and methods used in many studies. Here, indicate whether each material, system or method listed is relevant to your study. If you are not sure if a list item applies to your research, read the appropriate section before selecting a response.

Materials & experimental systems

| n/a | Involved in the study |
|-------------------------------------|---|
| <input checked="" type="checkbox"/> | <input type="checkbox"/> Antibodies |
| <input type="checkbox"/> | <input checked="" type="checkbox"/> Eukaryotic cell lines |
| <input checked="" type="checkbox"/> | <input type="checkbox"/> Palaeontology |
| <input type="checkbox"/> | <input checked="" type="checkbox"/> Animals and other organisms |
| <input checked="" type="checkbox"/> | <input type="checkbox"/> Human research participants |
| <input checked="" type="checkbox"/> | <input type="checkbox"/> Clinical data |

Methods

| n/a | Involved in the study |
|-------------------------------------|--|
| <input checked="" type="checkbox"/> | <input type="checkbox"/> ChIP-seq |
| <input type="checkbox"/> | <input checked="" type="checkbox"/> Flow cytometry |
| <input checked="" type="checkbox"/> | <input type="checkbox"/> MRI-based neuroimaging |

Eukaryotic cell lines

Policy information about [cell lines](#)

| | |
|---------------------|---|
| Cell line source(s) | Wildtype E14-IB10 mouse ES cells were obtained from E. R. Maandag (Nederlands Kanker Instituut). Bra::GFP mouse ES cells were obtained from the Keller's lab. Nodal::YFP mouse ES cells were obtained from the Collignon's lab. TCF/LEF mycherry mouse ES cells were obtained from the Hadjantonakis's lab. LfngT2AVenus mouse ES cells were obtained from the Aulehla's lab. |
| Authentication | For the Bra::GFP cell line: stimulation with Chiron induced expression of Bra::GFP in the posterior part of gastruloids. |

| | |
|---|---|
| Authentication | For the TCF/LEF line: stimulation with Chiron induced expression of the reporter in the posterior region of gastruloids. For the Nodal::YFP line we tested whether the reporter expression was blocked by the Nodal inhibitor SB43 and switched on by Nodal and Activin A. For the LfngT2AVenus line: gastruloids made from this line displayed dynamics very similar to previously described dynamics of the LuVeLu and LfngT2AVenus Notch-signaling reporters in mouse embryos (see Sonnen et al., Cell, 2018), and the signal disappeared upon application of the Notch inhibitor DAPT. Our RNA-seq experiments confirmed that all these cell lines were indeed derived from mice. |
| Mycoplasma contamination | All cell lines tested negative for mycoplasma contamination. |
| Commonly misidentified lines (See ICLAC register) | No commonly misidentified lines were used in this study. |

Animals and other organisms

Policy information about [studies involving animals](#); [ARRIVE guidelines](#) recommended for reporting animal research

| | |
|-------------------------|--|
| Laboratory animals | E8.5 mouse embryos used for tomo-seq were derived from crosses between CD-1 females and CD-1 stud males. |
| Wild animals | This study did not involve wild animals. |
| Field-collected samples | This study did not involve samples collected from the field. |
| Ethics oversight | All animal experiments for this project were approved by the Animal Welfare and Ethical Review Body for the University of Cambridge. Relevant Home Office licenses are in place. |

Note that full information on the approval of the study protocol must also be provided in the manuscript.

Flow Cytometry

Plots

Confirm that:

- The axis labels state the marker and fluorochrome used (e.g. CD4-FITC).
- The axis scales are clearly visible. Include numbers along axes only for bottom left plot of group (a 'group' is an analysis of identical markers).
- All plots are contour plots with outliers or pseudocolor plots.
- A numerical value for number of cells or percentage (with statistics) is provided.

Methodology

| | |
|---------------------------|---|
| Sample preparation | Gastruloids were washed with PBS 2x, incubated in Trypsin-EDTA at 37 °C for 5 min and titrated with a P200 pipette, after which ESLIF (serum + LIF medium) was added to neutralize the Trypsin. After centrifugation (200 x g, 3 min), cells were resuspended in PBS with 10% serum and filtered through a 35 µm filter (Falcon, 352235). Prior to FACS, DAPI (Thermo Fisher) was added to assess cell viability. For SORT-seq, individual live cells were sorted into the wells of a 384-well plate using a BD FACSJazz Cell Sorter (BD Biosciences) that was equipped with BD FACS software (version 1.2.0.124). For 10x genomics scRNA-seq, washes were done using PBS0 (PBS without calcium and magnesium), and 100,000 live cells were sorted into 1.5 ml DNA lowbind tubes (Eppendorf, 022431021) that were pre-filled with 50 µl PBS0. |
| Instrument | BD FACSJazzTM Cell Sorter (BD Biosciences); cat. no 655489. |
| Software | Flow cytometry data was collected and analyzed using BD FACS software (version 1.2.0.124). |
| Cell population abundance | The abundance of the cell population that was used for scRNA-seq is indicated in Extended Data Fig. 1a |
| Gating strategy | The gating strategy is shown in Extended Data Fig. 1a. |

Tick this box to confirm that a figure exemplifying the gating strategy is provided in the Supplementary Information.